ORGAN DECELLULARIZATION USED AS A NOVEL APPROACH TO ENGINEER THREE-DIMENSIONAL UROGENITAL TUMOR MODELS

by

Zheng Tan

B.Sc., Simon Fraser University, 2016

A THESIS SUBMITTED IN PARTIAL FULFILLMENT OF

THE REQUIREMENTS FOR THE DEGREE OF

MASTER OF SCIENCE

in

THE FACULTY OF GRADUATE AND POSTDOCTORAL STUDIES

(Experimental Medicine)

THE UNIVERSITY OF BRITISH COLUMBIA

(Vancouver)

June 2019

The following individuals certify that they have read, and recommend to the Faculty of Graduate and Postdoctoral Studies for acceptance, the dissertation entitled:

ORGAN DECELLULARIZATION USED AS A NOVEL APPROACH TO ENGINEER THREE-DIMENSIONAL UROGENITAL TUMOR MODELS

submitted by Zheng Tan in partial fulfillment of the requirements for the degree of Master of Science

in Experimental Medicine

Examining Committee:

Alan So, Urologic Sciences
Supervisor

Michael Cox, Urologic Sciences
Supervisory Committee Member

Karen Cheung, Electrical and Computer Engineering
Supervisory Committee Member

Vincent Duronio, Respiratory Medicine
University Examiner

Additional Supervisory Committee Members:

Claudia Chávez-Muñoz, Urologic Sciences
Supervisory Committee Member

Supervisory Committee Member

Abstract

Cancer is currently the leading cause of death in Canada and is responsible for 30% of all deaths (1). With various treatments available nowadays, it is necessary to develop a three-dimensional (3D) model to mimic *in vivo* condition of patients' disease in order to test drug efficacy prior to any actual treatments. My study is focusing specifically on kidney and bladder cancer. Therefore, a 3D, acellular organ-specific extracellular matrix (ECM) can be established as bioactive substrates with the long-range goal of bioengineering tumors for drug testing. Specifically, decellularization is the process by which cells are removed from the organ to produce the aforementioned matrix. It is crucial to achieve a tight balance between effective cell removal and retention of native ECM architecture. Henceforth, the decellularized matrix can be used as a template and be repopulated with normal human organ-specific cells or cancerous cells. With these approaches, a bio-matrix that ultimately serves as a cancer model for drug testing can be developed. In this master's thesis project, I hypothesized that decellularization preserves organ microarchitecture and retains various matrix-bound growth factors necessary for cell homing. Afterward, tumor models can be established through recellularization of human cells onto the decellularized ECMs as a proof-of-principle drug-testing platform to predict treatment response.

Two objectives were pursued to test this hypothesis. Under objective 1, I optimized and established decellularization protocols for both kidney and bladder. The protocols ensure complete cell removal and preservation of ECM microarchitectures. In addition, comprehensive protein-profiling of the decellularized kidney and bladder's ECM was completed by performing proteomic analysis with liquid chromatography–mass spectrometry (LC-MS/MS). Under objective 2, recellularization protocols for both decellularized kidney and bladder ECM were established and optimized. As the decellularized kidney and bladder's ECM was repopulated with normal human cells and cancerous cells, the proposed *in vitro* urogenital cancer model can be developed.

In conclusion, a 3D *in vitro* urogenital cancer model can be developed from kidneys and bladders using protocols optimized under objective 1 & 2. This work establishes the model as proof –of principal and sets the foundation for the developments of personalized cancer treatments.

Lay Summary

Current and future management of kidney and bladder cancers ideally will be based on choosing the optimal treatments for each patient, potentially from many options. It is necessary to develop cancer models to mimic the condition of patients' disease in order to test drug efficacy prior to any actual treatment. To obtain these models, we obtained kidneys and bladders from animals, removed all cellular components from each organ while the organ's inside structure remained intact. Afterward, these cell-free organs can be repopulated with normal human organ-specific cells or cancerous cells. The repopulated organs could ultimately serve the purpose of mimicking patients' disease. Therefore, building these models may allow healthcare providers to use patients' own cells to create replicas of their urogenital tumors. Hence, multiple drug tests can be performed on this clinical platform instead of on the patient to prevent unnecessary side effects.

Preface

The content presented in this thesis is the original and unpublished work written by me with extensive review by Dr. Alan So, Dr. Claudia Chávez-Muñoz, Dr. Michael Cox, and Dr. Karen Cheung.

All experiments were designed and supervised by Dr. Alan So and Dr. Claudia Chávez-Muñoz and performed by me, with assistance from Dr. Gethin Owen, Dr. Igor Moskalev and Mr. Hans Adomat for Scanning Electron Microscope (SEM), animal organ retrieval and LC-MS/MS. All animal procedures were conducted according to the guidelines and principles of the Canadian Council on Animal Care (CCAC). The organ retrieving protocol was approved by the Animal Care Committee of the University of British Columbia (Protocol No. A18-0203).

Table of Contents

List of Tables

List of Figures

List of Abbreviations

ACN – Acetonitrile

ccRCC – Clear cell renal cell carcinoma

DAB – 3,3'- diaminobenzidine

dH_2O – Distilled Water

ddH_2O – Double Distilled Water

DMEM - Dulbecco Modified Eagle Medium

DNA - Deoxyribonucleic Acid

DNase I - Deoxyribonuclease I

DTT - 1,4-dithiothreitol

EBM™- Plus - Endothelial Cell Growth Basal Medium-Plus

ECM - Extracellular Matrix

EnGS – Endothelial Growth Supplement

FBS - Fetal Bovine Serum

HCD – higher-energy collisional dissociation

H&E - Hematoxylin and Eosin

HRP – Horseradish Peroxidase

IHC – Immunohistochemitry

KSFM - Keratinocyte Serum Free Medium

LC-MS/MS - Liquid chromatography–Mass spectrometry

MEM - Minimum Essential Medium Eagle

MIBC - Muscle Invasive Bladder Cancer

m/z – mass/charge ratio

PBS - Phosphate-buffered saline

PDX - Patient-derived tumor xenografts

PNGase F - Peptide-N-Glycosidase F

rhEGF - Recombinant human epidermal growth factor

RNAse A - Ribonuclease A

SDS – Sodium Dodecyl Sulphate

SEM - Scanning Electron Microscope

TBS – Tris-buffer Saline

TFA – Trifluoroacetic acid

TURBT - Transurethral Resection of Bladder Tumor

USP - United States Pharmacopeia unit

2D – Two Dimensional

3D – Three Dimensional

Acknowledgements

First and foremost, I would like to express my sincere gratitude to my supervisor Dr. Alan So for giving me this precious opportunity to start my career in research. I would not have developed this much passion and determination in this field without his learned guidance and tireless support. Even I am a student with many flaws, he tolerated me and guided me to the right directions. I would also like to thank Dr. Claudia Chávez-Muñoz for guiding me through every steps of my study with her extensive knowledge and experiences. She is always a phone call away when I have questions, concerns, or need assistance and even for pep talks. It is a privilege to have her with me for the past three years. I appreciate her intelligence and admire her as an omnipotent sister.

I am very grateful to my supervisory committee member, Dr. Michael Cox. He teaches me how to think critically in both research and life. I appreciate him being straightforward and I am impressed by his sense of humor. He never knows how his voice cheers me up when I am in the doldrums. Dr. Karen Cheung, my other committee member, I want to thank her for being there monitoring my research progress and I sincerely appreciate her technical support even before I started my master's study. I appreciate that she introduced me to her lab and provided me a valuable opportunity to learn from her students. That was how I get to know biomedical engineering at the first place. I would also like to thank Dr. Caigan Du, who is a mentor

to me for the past three years. I appreciate that although I am not one of his students, he still spent so much time encouraging and enlightening me with his big heart and formidable vision. He influenced me in aspects that even himself didn't notice. Lastly, I would like to express my deepest gratitude to my parents, grandparents and aunt for their unconditional love and trust.

I am fortunate enough to have everyone mentioned above during my study. I would never have learned the beauty and fascination of scientific research without them being around.

Dedication

To my dearest parents.

Chapter 1: Introduction

1.1 Urogenital cancers

1.1.1 Kidney cancer

Kidney cancer is the tenth most commonly diagnosed cancer in Canada. The incidence of kidney cancer in Canada has increased by approximately 1.3% per year for both genders since the late 1990s (2). In 2017, there were approximately 6,600 Canadians were newly diagnosed and 1,900 died from this malignancy (1) (3). Patients presenting with localized kidney cancer are usually initially treated with partial/radical nephrectomy. Resected tumors are assessed pathologically for both grade and stage and this information provides prognostic information and directs further management. Medical management options in addition to surgery include targeted therapy, immunotherapy, radiation therapy or a combination of these (2). However, identification of the optimal medical procedures is considered challenging and inappropriate decision can cause additional side effects to patients.

1.1.2 Bladder cancer

Bladder cancer is the fifth most commonly occurring cancer in Canada. Due to its high recurrence rate (60-70%), bladder cancer is the most expensive cancer to treat (4). In

2017, approximately 8,900 Canadians were newly diagnosed and 2,400 died from this malignancy (1). Patients presenting with bladder cancer are initially treated with transurethral resection of bladder tumor (TURBT). Tumors are assessed pathologically for both grade and stage and this information provides prognostic information and directs further management. In bladder cancer, chemotherapy is frequently administered neoadjuvantly in patients undergoing radical cystectomy for pT2 (patient with stage II, invasion of the muscle) bladder cancer, but identification of those with chemo-sensitive cancer is challenging.

1.1.3 Clinical limitations

Current treatment limitations in both kidney and bladder cancer center on the inability of predicting optimal treatments from a large myriad of possible options; hence, identifying drug sensitivities prior to treatments would allow for a more efficacious management with minimal delay that may be caused by using therapies in which the tumors have inherent treatment resistance.

Therefore, current and future management of kidney and bladder cancers ideally will be based on choosing the optimal and treatment-sensitive approach for each patient potentially from a vast array of options. In order to study the variable response to treatment secondary to interpatient heterogeneity and, more importantly, translate this knowledge into true patient benefit, predictive tumor models provide an opportunity to guide individual treatment and identify tumor-specific optimal therapies. However,

many existing models do not necessarily fulfill these requirements due to many limitations that restrict their predictive power (5).

1.2 Current available models

1.2.1 Two-dimensional tissue models

Currently, many tumor models play important roles in cancer research and serve as screening platforms for drug testing. For both *in vitro* and *in vivo* tumor models, there are needs for improved understanding of not only cancer progression but also prediction of the cancer's response to therapies.

The typical representative *in vitro* model uses an adherent two-dimensional (2D) monolayer cell culture. In this model, cancer cells are continuously cultured and adapted to *in vitro* cell culture conditions. Consequently, this model is well established and has plenty of previous experimental data to compare with. The model is cost effective and also easy to visualize and analyze. However, the 2D model is not a representative of actual cell microenvironment due to low physiological relevance, such as the lack of true tissue architecture and cell-cell communication. Cancer cells cultured in 2D monolayer exhibit different cellular morphology, metabolism, and gene expression compared to those *in vivo* (6) (7) (8). Hence, 2D cell models do not mimic the complex cellular interactions and as such studying either normal or malignant cells using this model may not be true representations of either canonical or malignant

biologic pathways. In other words, 2D models are not optimal tools as a preclinical cancer model.

1.2.2 Three-dimensional tissue models

a) Co-culture models

Three-dimensional (3D) *in vitro* models such as co-cultured tumor models and spheroid tumor models attempt to emulate the complexities of cell-cell interactions *in vitro*. 3D cultures can, in contrast to 2D monolayers, have higher degree of structural complexity and retain cell-cell and cell-matrix interactions that better reflect the characteristics of normal and malignant tissue (7). Therefore, 3D models better simulate true biologic conditions.

Co-culture tumor models are developed to have cancer cells cultured with a variety of stromal cells, with which the model can apply stromal-mediated effects that are found within *in vivo* cancer tissue (9) (10). Unlike 2D monolayer models wherein different cell types are mixed and cultured on the same monolayer, the co-culture model system allows different cells to be cultured in different compartments or matrix layers. Stromal cells and cancer cells can be co-cultured in separate 3D layers to mimic different components in the tumor microenvironment. However, the models are complex to grow and lack sufficient extracellular matrix (ECM) as that of *in vivo* conditions; they are also challenging to be used in a high-throughput manner and cells in co-culture models are difficult to detect and quantify at the end of the study (11). In

addition, the absence of ECM inhibits cancer cells from invading or metastasizing to surrounding tissues due to lack of cell-ECM interactions (12). Hence, co-culture model is not an optimal tool to study cancer cell behaviors.

b) Spheroid models

Spheroid tumor model aggregates cells grown in suspension or embedded in a 3D matrix using 3D culture methods such as suspension in culture, non-adherent surface methods, hanging drop methods, and microfluidic methods (13) (14) (15) (16). Larger spheroids sustain nutrient and oxygen level differently throughout the spheroid that usually result in the formation of a necrotic core (17), which is similar to poorly vascularized *in vivo* tumors. Moreover, protein and gene expression profiles of cancer cells in spheroids also more closely resemble those found in clinically and *in vivo* models better than 2D models (13). These features make the spheroid tumor models more biomimetic than the co-culture tumor models. However, spheroid tumor models produced with the aforementioned four methods have different limitations. Spheroids maybe developed with uniformity in size but this is not usually done in a high-throughput manner (i.e. non-adherent surface methods and hanging drop methods). Conversely, other protocols do produce spheroids in a high-throughput manner with little control of sizes and uniformity (i.e. suspension in culture method) (13) (14) (15) (16). Other spheroid tumor models may be produced with extrusion 3D bioprinters. Normal and cancerous cells as well as matrix can be positioned one by one within a 3D architecture to drive the formation of tumor spheroids. This model is considered a heterogeneous tumor model and it mimics the true cellular density of target tissues

and organs (18). However, shear-stress-induced cell deformation can occur during bioprinting and potentially cause apoptosis afterward (19). Similar to that of the co-culture models, the major limitation of the spheroids models is the matrix. Even though cells in spheroids are in a matrix instead of co-cultured or cells attached to plastic, the matrices are usually synthetic or only collagen, fibrin or hyaluronic acid (20) (21). They do not have the complexity of natural mammalian ECM. In this case, the “less sophisticated” ECM could inhibit cancer cells from invading or metastasizing to surrounding tissues due to lack of cell-ECM interactions (12), which could lead to partial or false translation of certain cancer cell behaviors.

1.2.3 Animal models

Animal or *in vivo* tumor models may be the ideal model to assess clinical efficacy of various treatments. Despite differences between human and animal biology, *in vivo* models capture the high degree of complexity of tumor biology in a living system, but have limited utility in imaging and high-throughput studies. A wide range of animal-based tumor models have been developed of tumors, including environmentally induced models, patient-derived tumor xenografts (PDX) models and genetically engineered mouse models (22) (23). The most studied predictive tumor model is the PDX model, in which cancer cells obtained from patients are implanted into immunocompromised mice and grown. These tumors can then be tested using various therapeutics to identify optimal treatments for the specific patient’s tumor (24) (25) (26). Although usually grown in rodents, the *in vivo* model best mimics the original

tumor environment. However, this model is very expensive and requires tremendous resources. These limitations have also restricted these models to research study and have prevented their practical clinical use in high-throughput drug screens (27). Therefore, a better more suitable tumor model is required, capable of **1)** predicting response to therapies; **2)** being cost-effective and reproducible; and **3)** having high-throughput approach.

1.3 Tissue engineering as an alternative study model

Overall, my aim in this study is to establish an economical and reliable high-throughput drug-screening platform. My study proposed to develop the foundation of a 3D *in vitro* patient-derived urogenital tumor model as a potential preclinical platform for drug testing. Therefore, in order to develop such tumor models that are potentially capable of predicting response to therapies, rodent/porcine kidneys and bladders were collected from animals being euthanized for other research projects that did not compromise the structural and functional integrity of either organs. With collection of these organs, it is essential to decellularize and recellularize them into ready-to-use models that are capable of mimicking the patient's diseases. The rationale of engineering an animal organ into a patient's disease model required techniques of tissue engineering.

In general, tissue engineering is a combination of the principles and methods of life sciences with that of engineering, to develop material and methods to replace

damaged or diseased tissues, and create entire tissue replacements (28) (29). The triad of tissue engineering are biomaterial/scaffold, cells and growth factors/bioreactor. The scaffold in tissue engineering provides 3D structure for cells to grow, proliferate and delivery biomolecules such as growth factors, cytokines, etc. (30). Growth factors are soluble proteins that stimulate cells in order to proliferate, migrate and differentiate (31) (32). Moreover, a bioreactor provides physical stimulation and condition for cell proliferation.

In my study, I aim to transform an animal organ/tissue into a tissue engineered scaffold to home normal cells and cancer cell lines in later procedures to simulate a certain disease. In order to home these new cells, cells from the animal organ are required to be completely eliminated first. Compared to synthetic matrices, the animal organ scaffolds are already biocompatible, biodegradable, vascularized and have mechanical properties that are suitable for cell growth. In summary, the principle is to remove previous resident cells and leave the ECM with preserved micro-architectures and composition.

1.4 Decellularization as a method for tissue engineering

In order to achieve the tight balance between complete cell removal and the integrity of ECM micro-architecture, a methodology called decellularization can be applied. Decellularization is the process used in biomedical engineering to isolate the ECM of a tissue from its inhabiting cells, leaving the ECM scaffold of the original tissue, which

can be used in artificial organ and tissue regeneration (33) (34) (35). Decellularization process can be accomplished through perfusion or immersion. As long as the tissue/organ is completely decellularized, other procedures for creating the tumor model can be applied.

1.5 Recellularization as a method for tissue engineering

With the completion of decellularization, resident cells are eliminated and the ECM microarchitecture was preserved. In order to engineer a model that mimics human tissue base on this scaffold, human cells can be reseeded into the decellularized ECM at correct position according to the nature of different cells. Recellularization is achieved as cells proliferating and growing in the matrices under appropriate culturing conditions.

1.6 Hypotheses and objectives

With the aforementioned principle and methodologies, I hypothesized that my decellularized ECM model has more clinical relevance to represent *in vivo* conditions compared to other models and it is able to retain various matrix-bound growth factors that may participate in cell homing. That being said, organ decellularization can be used to develop a high throughput urogenital tumor model resembling patient's tumor environment.

There are two objectives in my study:

1) To establish kidney and bladder decellularization methodology including characterization and evaluation of the decellularized ECMs.
2) To recellularize the decellularized ECMs with different human normal cells or cancerous cells to create a tumor model.

With these two objectives, I aim to establish a novel 3D clinical platform that can potentially predict treatment outcomes of urogenital cancers. This would be the first test-model that utilizes human cell lines to study the accessibility and cellular behavior of urogenital cancers in an environment that mostly mimics that of *in vivo* conditions. Overall, I am hoping that this study will set the foundation of a new preclinical tumor model that will significantly impact the way clinicians treat patients with kidney and bladder cancers. This study could potentially give a clue to researchers who want to generate engineered 3D patient-derived models that accurately recreate the urogenital tumor of an individual patient. Developing this 3D *in vitro* cancer model may allow us to potentially use patient's own cells to create a replica of the patient's tumor; this model may then provide the ability to perform multiple drug tests on this clinical platform and thus potentially allow healthcare providers to simultaneously screen multiple anti-cancer drugs in an individualized manner *ex vivo*. This model potentially avoids the need to sequentially use ineffective therapies in a patient to prevent unnecessary side effects and costs. If successful, the engineered 3D patient-derived urogenital cancer model will allow healthcare providers to identify the most efficacious therapy and will lead to the improvement of the patient's overall survival and quality of life.

Chapter 2: Materials and Methods

2.1 Organ retrieval from animals

a) Kidney retrieval

Prior to organ collection from rodents, intracardiac injection of heparin (200 USP in 800 µL of Phosphate-buffered saline) (Fresenius Kabi, sodium injection, C504730, Bad Homburg, Germany) was performed to introduce systemic distribution of anticoagulant to prevent thrombosis in organs. To perform intracardiac injection of heparin, 1 mL syringes were loaded with heparin (1000 USP units/mL) and set aside for later use. Under overdose of anesthesia, rodents were placed in dorsal recumbency and pedal reflexes were checked to ensure that they were deeply anesthetized. After the needle tip was through the skin, syringe plunger was pulled slightly to create negative pressure and then advanced until blood was drawn into the syringe. Heparin is then infused over 1 minute to allow circulation throughout the body. Once heparin injection was completed, euthanasia was initiated. Euthanasia consisted of two steps: **a)** overdose of isoflurane (5% flow rate concentration or greater) followed by **b)** cervical dislocation.

For kidney retrieval: immediately after euthanizing the rodents, the abdominal cavity was opened and the aorta was dissected to the renal artery. After that, the celiac, splenic and mesenteric arteries as well as renal vein were ligated with 5-0 Ethilon

nylon suture (Ethicon, GA, USA) leaving patent the renal artery and the ureter. A 24-gauge catheter (Becton, Dickinson and Company, 382512, NJ, USA) was placed in the aorta toward the renal artery with 1000 units of heparin perfused through the catheter (perfusion time was around 1 minute). As fading of the red-brown color of the kidney confirmed proper placement of the catheter, ligature was tightened to hold the catheter in place. All other connected vessels were ligated and removed. Once the kidney was detached, it was placed in 20 mL of phosphate-buffered saline (PBS) with 100 units of heparin and a 10 mL syringe containing the same solution was attached to the catheter. Small amount of solution was drop-wisely perfused every 2 - 3 minutes to wash out the blood from the organ. The kidney obtained and processed to this point would be ready to use for decellularization. The kidney – catheter system was kept on ice.

Important aspects of organ harvesting should be mentioned: **1)** Perfusion of heparin should be very slow and gentle to prevent the flimsy renal capillaries from bursting. **2)** Saline should be instilled in the abdominal cavity when kidney is exposed to air to prevent desiccation. If working with one kidney at a time, the contralateral side should be wrapped with saline moist gauze to prevent damage of kidney during exposure in air. **3)** Placement of the catheter must be done carefully as this step may damage the arterial lumen to prevent infusion. Minimal attempts of catheter placement should be performed. **4)** Infusion of heparin must be started quickly to prevent thrombosis in the small caliber vessels, which would make them unable to achieve complete decellularization and thus not a good candidate for future experiments. Therefore, the

aforementioned precautions during dissections are vital for us to obtain eligible starting materials for the upcoming decellularization procedures.

b) Bladder retrieval.

The rodent bladder retrieval was performed subsequent to kidney retrieval. A midline incision from the xiphoid process to the pubic symphysis was made and the urinary bladder would usually be located in the lower center of the abdomen close to the pelvic bone. Both ureters and the urethra were ligated with silk suture and then divided and then the bladder was dissected from the animal.

For porcine bladder retrieval, animals were euthanized under corresponding primary research protocol, which can be an overdose of injectable anesthetic. Immediately after euthanizing the pig, the abdominal cavity was opened with a midline incision and then the bladder was identified. The porcine bladder, which is long and flat, can be found between the blood vessels in the umbilical cord. The bladder was then cut into multiple 1 cm × 1 cm × 0.5 cm pieces to obtain greater surface area during decellularization and were placed in PBS solution (on ice) immediately. The size of each pieces is similar and thus could be used as experimental replicates in future procedures.

2.2 Decellularization protocols

2.2.1 Background

Since the success of decellularization were mainly relied on four aspects **1)** the original conditions of the organs **2)** performance during organ dissections **3)** parameter settings of the peristaltic pump during kidney perfusion/cycle controls during bladder immersion and **4)** the sterilization of the experimental organs during decellularization. Any inconsistencies in between would cause failure or inefficiency of decellularization and ended up with wasted organs, of which consequences deviate from our original intention to reduce animal usage. In worse cases, the failure or inefficiency during decellularization was not prominent enough to observe and the organs were proceeded to following recellularization procedures. It could end up with flawed tumor models that are not representatives of human conditions and could possibly provide false therapy suggestions to patients. Gender was not considered an issue for my study and diseases/treatments applied to the animals needed to be evaluated individually, since some may or may not alter the physiological condition of the organs. Perfusion and immersion decellularizations were both performed under sterile condition in this study. Whole kidney decellularization was performed with perfusion and decellularization of bladder pieces were performed with immersion (Figure 1).

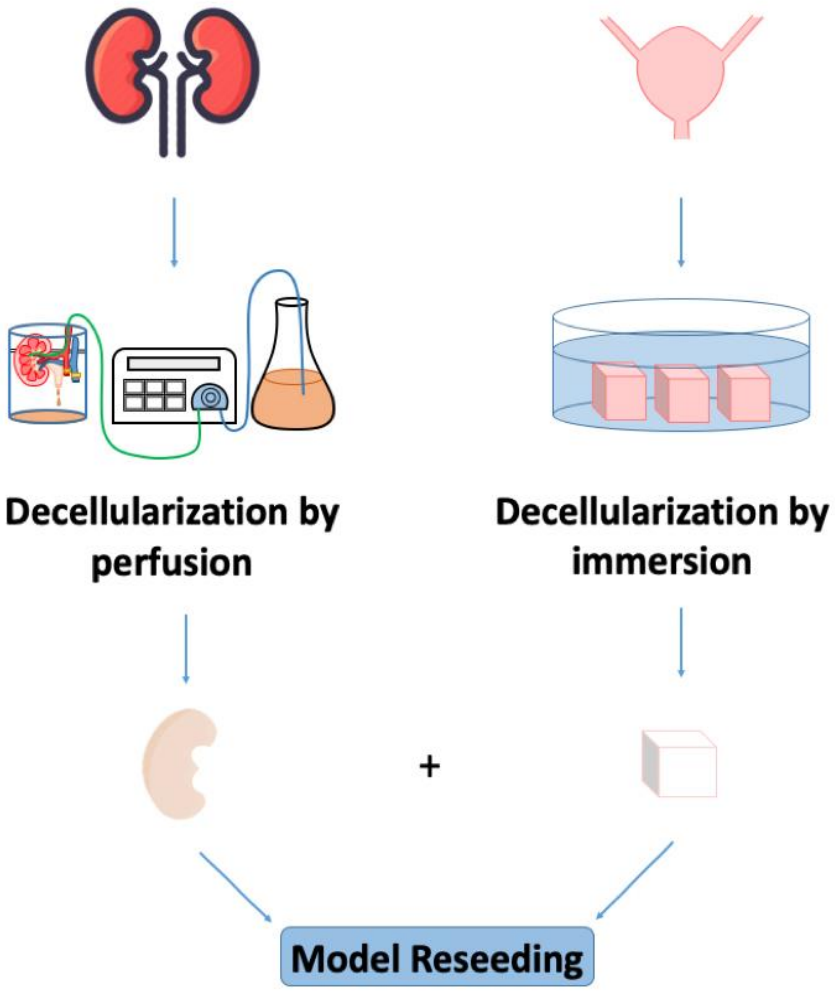

Figure 1. Decellularization protocols. Two decellularization strategies: decellularization by perfusion in a bioreactor with a peristaltic pump (kidney) and decellularization by immersion (bladder).

2.2.2 Bioreactor

An in-house developed perfusion-based bioreactor was constructed with an airtight polycarbonate food container which is BPA-free, has a volume of 3-quart with silicone gasket. Three holes were drilled on the container (Figure 2) and they were insulated with three lure-lock connecters. The top two connecters were attached with a needle-free IV connectors & catheter extension set, respectively. Inside of the bioreactor, a stainless-steel rod was inserted and glued onto the upper inside wall and two hooks were hanged on it. This system would be able to suspend the organ with attached catheter and could keep balance of the organ during perfusion. A peristaltic pump was connected to the set and could perfuse solutions into the bioreactor. The bottom connecters were attached to a needle-free IV connecter only and could release used solutions.

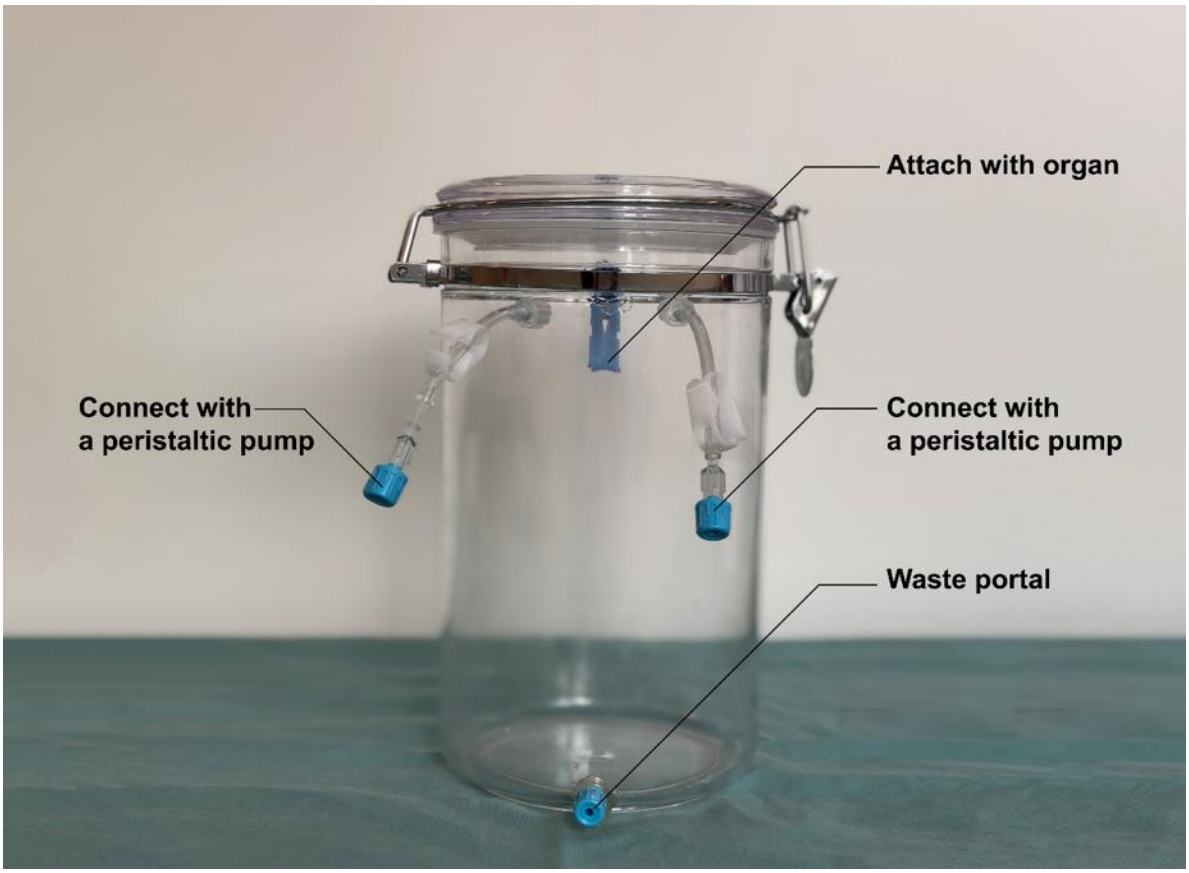

Figure 2. The bioreactor used for kidney decellularization (perfusion).

2.2.3 Decellularization by perfusion – kidney.

At room temperature, the rodent kidney was placed inside of the bioreactor described in section 2.2.2 and the catheter previously inserted in the renal artery was connected to a peristaltic pump (Braintree Scientific, BS-900 programmable peristaltic pump with 4 roller pumping head & 1/16 ID tubing, MA, USA) to allow continuous passing through of different solutions from the inserted catheter (Figure 3). The whole system of the peristaltic pump including all tubes and the bioreactor were sterilized with 70% ethanol beforehand or the kidneys would end up with bacterial or fungal contamination. The kidneys need to be securely placed in the bioreactor because peristalsis could possibly push the kidneys down and disconnect the catheter during perfusion.

Since one of the 1% Triton X-100 solution perfusion cycles was overnight, it is crucial to immobilize the kidneys with an extra ligature tied with the hook hanged on the stainless rod to prevent them from falling down (Figure 4). On the other hand, the peristaltic pump needs calibration for each usage since it was found that the flow rate could vary to some extent from time to time. The ideal way to minimize this mechanical error is to measure the actual flow rate before perfusion of the kidneys. The pump could be turned on for five to ten minutes beforehand and the amount of solution being passaged was measured. With this approach, the actual flow rate could be calculated and thus certain adjustments could be applied to the pump parameter settings.

Distilled water (dH2O) was perfused at a flow rate of approximately 5 mL/min for 200 minutes in total to eliminate remaining blood cells. 1% Triton X-100 solution (Fisher Scientific, BP151, PA, USA) was perfused at the same rate for 400 minutes in total. The same solution would then be perfused at a rate of approximately 1 mL/min for 1000 minutes in total. Finally, 0.1% sodium dodecyl sulphate (SDS) solution (Fisher Scientific, BP1311, PA, USA) was delivered at a flow rate of approximately 5 mL/min for 200 minutes in total. The above cycle can be repeated for 2 – 3 time depends on the size and volume of the organ. At the end of the last cycle, the kidney was perfused with dH2O for 24 hours followed with perfusion of Deoxyribonuclease I (DNase I, 2,000 units) (Sigma-Aldrich, D4513, MO, USA) for 120 minutes. Afterward, additional perfusion with dH2O was performed for 4 - 5 days at a flow rate of approximately 1 mL/min (5760 to 7200 mL in total) to eliminate any remaining detergents/chemicals in the kidney.

During perfusion, it is observed that the kidneys were not blanching much (still have brown color) within the 1% Triton X-100 cycles but turned almost translucent during the short 0.1% SDS cycle. It is because Triton X-100 solution disrupts DNA-protein, lipid-lipid and lipid-protein interaction (35) whilst maintaining native protein structures. SDS solutions completely solubilize cell and nucleic membranes and fully denature proteins (36). Structural proteins of kidneys were not supposed to be disrupted in this study and that is the reason why 0.1% SDS cycle is much shorter than the 1% triton X-100 cycle. On the other hand, the original size of the dissected kidneys is also

crucial. Larger animals usually have larger kidneys and larger kidneys always require more perfusion cycles to ensure complete decellularization.

Other earlier tested protocols can be found in appendix A & C.

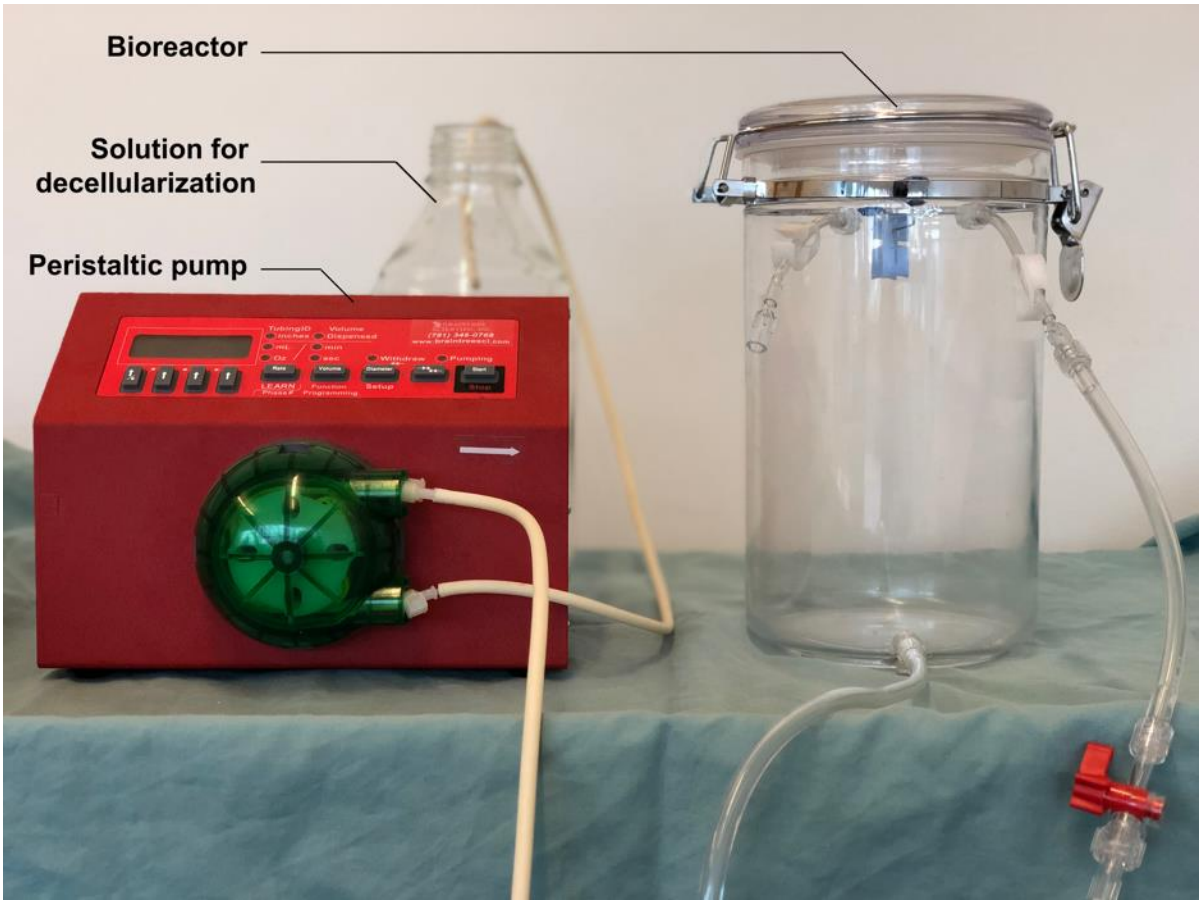

Figure 3. The bioreactor-peristaltic pump set up for kidney decellularization (perfusion).

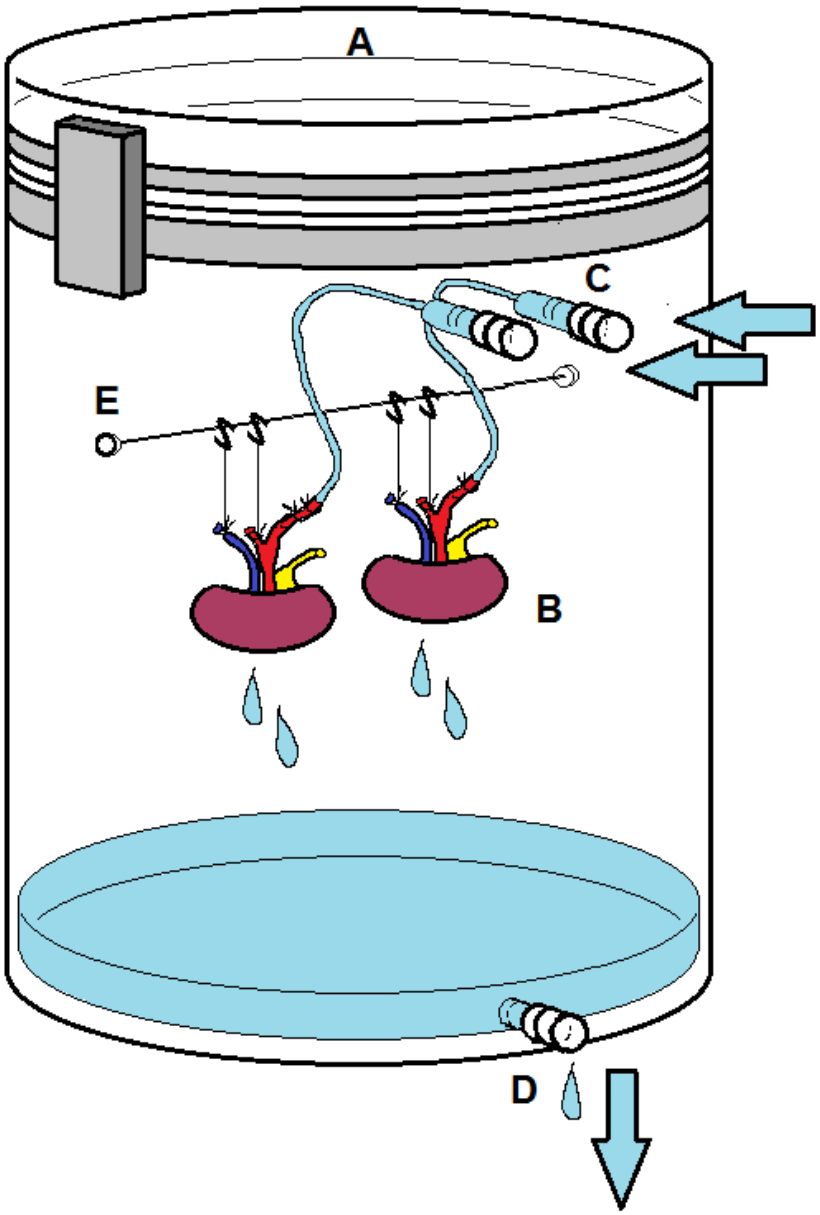

Figure 4. The schematic diagram of the bioreactor used for kidney decellularization (perfusion). (A) Sealed top of the bioreactor. **(B)** Kidneys during decellularization. **(C)** Peristaltic pump connecting portals. **(D)** Waste portal. **(E)** stainless-steel rod glued to the inside wall of the bioreactor to support kidneys.

2.2.4 Decellularization by immersion – bladder

Bladders were collected and processed as described in section 2.1 (b). Immediately after collection, bladders were immersed in Dulbecco Modified Eagle Medium (DMEM) (Fisher Scientific, 13345364, PA, USA) with 50 nM Latranculin B (Cayman Chemical, CAS 76343-94-7, Michigan, USA) and incubated for 120 minutes at 37ºC. After incubation, tissues were transferred into sterile dH2O at room temperature and they were agitated on a shaker for 15 minutes, making one change of sterile dH2O and agitating for another 15 minutes. Afterward, tissues were immersed in sterile 0.6 M potassium chloride solution (Fisher Scientific, AC424090010, PA, USA) at room temperature and were agitated on a shaker for 120 minutes. Then, tissues were immersed in sterile 1 M potassium Iodide solution (Sigma-Aldrich, 03124, Darmstadt, Germany) at room temperature and were agitated on a shaker for 120 minutes. Finally, tissues were immersed in sterile dH2O at room temperature overnight. The above described steps were considered one full cycle. Each cycle was repeated 10 - 12 times depending on size and volume of the tissue to ensure proper decellularization. Tissues were then incubated in DNase I (1 kU/mL; Sigma-Aldrich, D4513, MO, USA) for 120 minutes. Finally, tissues were washed in dH2O for 2 days with daily water changes to remove remaining reagents. 150 mm x 25 mm tissue-culture treated culture dishes (Sigma-Aldrich, CLS430599, Darmstadt, Germany) were used for bladder immersion decellularization.

Each solution used for bladder immersion decellularization are prepared in sterile conditions (including dH2O) and solution changes between each immersion cycles should also be performed in a sterile biosafety cabinet to reduce the risk of bacterial or fungal contamination. Larger petri dishes (150 mm x 25 mm in size) were used for agitation in order to obtain stronger centrifugal forces. Also, there were no more than five bladder pieces in each petri dish to ensure sufficient movement when agitated.
In general, porcine bladder immersion involved fewer complex procedures compared to that of rodent kidney perfusion. Porcine bladders are less delicate than kidneys and thus are easier to handle.

Other earlier tested protocols and rationales can be found in appendix B.

2.3 ECM evaluation

Decellularization protocols were evaluated from several aspects. Since the success of each protocol was determined on the extent of cell removal and the preservation of ECM microarchitecture, I evaluated the ECMs with three approaches: macroscopic visualization, Deoxyribonucleic acid (DNA) quantification and histological assessments including hematoxylin and eosin (H&E) stains and visualization with scanning electron microscope (SEM).

2.3.1 DNA quantification

Both native and decellularized organ/tissue were cut up to 25 mg pieces prior to DNA extraction procedures. The small pieces were digested individually using Proteinase K (QIAGEN, 19133, Hilden, Germany) at 56ºC with agitation until they were completely lysed. DNA was distracted and purified using the DNeasy Blood & Tissue Kit (QIAGEN, 69504, Hilden, Germany) according to the manufacturer's instructions. Briefly, upon removal of RNA, DNA samples were isolated by spin column-based nucleic acid purification procedures. Afterward, both native and decellularized tissue's DNA extracts were quantified spectrophotometrically using NanoDrop technology (Thermo Scientific, ND-2000, MA, USA). This approach of DNA quantification was to determine how thorough the decellularization protocol was and according to previous publications (37)**,** it is proved with a destructive method that less than 5% of DNA remnant/less than 50 ng of double strand DNA in 100 mg of decellularized tissues compare to that of native tissue considered successful decellularization (38). The unpaired (Two Sample) t test was performed to assess speculated changes.

2.3.2 Histological assessments

a) H&E

To assess cell removal and the preservation of ECM microarchitecture of the decellularized tissues, H&E stain was performed to both native and decellularized tissues. All tissues were fixed overnight in 1:10 dilution neutral buffered formalin (10%

formalin) (Fisher Scientific, 22-046-361, PA, USA) and then transferred to 70% ethanol prior to paraffin embedding, sectioning and staining. First, tissues were serially dehydrated in 70% (30 minutes), 80% (120 minutes, two changes), 95% (120 minutes, two changes) and 100% ethanol (90 minutes, three changes). Following dehydration, tissues were immersed in two xylene solutions to for clearing: **a)** Immersed in 100% ethanol and 100% xylene solution (1:1) (Sigma Aldrich, 534056, Darmstadt, Germany) for 30 minutes then **b)** immersed in 100% xylene for 30 minutes. With completion of these steps, all tissues were embedded into paraffin blocks and sectioned into 5 µm thickness. Sections were baked at 37 °C overnight prior to deparaffinization and rehydration. For deparaffinization, the sections were immersed in CitriSolv hybrid solvent and clearing agent (Fisher Scientific, 22-143-975, PA, USA) for 5 minutes (repeated three times). Sections were then serially rehydrated in 100%, 95%, 80% and 70% ethanol solution for 3 minutes each (with two repeats for each step) and were immersed in dH_2O for 5 minutes with three repeats. Afterward, the sections were stained with hematoxylin solution, Gill No.2 (Sigma Aldrich, GHS232, Darmstadt, Germany) for 3.5 minutes and rinsed with tap water followed with immersion in Shandon bluing reagent (Thermo Fisher, 6769001, MA, USA) for 30 seconds. The sections were again rinsed in tap water and stained with Eosin Y-solution (Millipore Sigma, 1098441000, Darmstadt, Germany) for 30 seconds. Another tap water rinse was performed prior to the serial dehydration afterward. The sections were dipped 10 times in 70%, 80% and 95% ethanol each and followed with two 1-minute immersion in 100% ethanol. At the end, sections were immersed in xylene for 3 minutes with three repeats and mounting solution was added prior to

cover-slipped visualization. The slides were then scanned with Leica SCN400 slide scanner (Meyer Instruments).

b) SEM

A segment of both native and decellularized kidney was primarily fixed in 4% paraformaldehyde (Electron Microscopy Sciences, 15710, PA, USA) in 0.1 M PIPES (Sigma-Aldrich, P6757, Darmstadt, Germany) buffer at room temperature for 10 hours, the pH was titrated down to 7.4. The tissue was briefly rinsed with the same buffer prior to the fixation in 2.5% glutaldehyde (Electron Microscopy Sciences, 16020, PA, USA) in 0.1 M PIPES buffer at room temperature for 20 hours, the pH was titrated down to 7.4. Tissue was then rinsed three times in the same buffer for 1 hour each, it was fixed in 1% Osmium Tetroxide (OsO_4) (Electron Microscopy Sciences, 19150, PA, USA) in 0.1M PIPES buffer, pH 6.8 at room temperature for 5 hours. Alter fixation, tissues were rinsed three times with double distilled water (ddH_2O) for 1 hour each. After rinsing, the specimen was dehydrated at room temperature in a graded ethanol-water series: 50%, 60%, 70%, 80%, and 90% solution for 1 hour each, followed with three times 100% ethanol (Electron Microscopy Sciences, 15056, PA, USA) for 1 hour each. Critical point drying using CO_2 (Tousimis Samdri®-795 critical point dryer) was applied for 1 hour to the specimen to ensure absolute dehydration and the specimen was finally mounted on an aluminum stub using sticky carbon tapes. The specimen on the stub was then coated with a thin layer of Au/Pd coating (2 nm thickness) using the Leica EM MED020 Coating System. Same sample preparation strategies were

performed to native and decellularized bladders. Images were recorded with a Helios NanoLab 650 Focused Ion Beam SEM.

2.4 ECM characterization

Other than the evaluation of complete cell removal, proteomics analyses were performed as a novel approach to determine the full protein profile of the decellularized organs (kidney and bladder) in this study. Current methods evaluating the completeness of organ decellularization are based mainly on the elimination of nucleic acids since they are easy to quantify. However, other structural and cellular materials, such as proteins are also essential in indicating the preservation of ECM. Therefore, additional characterization, such as proteomic analyses, will provide molecular readouts of the composition of decellularized kidney and bladder ECM scaffold.

A compartment protein extraction kit (Millipore Sigma, 2145, Darmstadt, Germany) was used to isolate subcellular and structural proteomes from the decellularized organs. This kit was also used to perform enrichment of some low-abundant proteins for further proteomic analysis using liquid Chromatography-Tandem Mass Spectrometry (LC-MS/MS). The procedures were followed according to manufacturer's instructions.

a) ECM protein extraction and enrichment

Before starting, a cocktail of protease inhibitor (provided with the compartment protein extraction kit) was added to all reagents/buffers from the kit to make it a 1X solution. All reagents and tissue samples were kept on ice for the duration of the processing and the only exception was the buffer CS, which was kept at room temperature to prevent SDS (used in decellularization) precipitation. According to the manufacturer's manual, the composition of buffers used in this experiment was provided:

Buffer C	HEPES (pH 7.9), MgCl2, KCl, EDTA, Sucrose, Glycerol, Sodium OrthoVanadate
Buffer W	HEPES (pH 7.9), MgCl2, KCl, EDTA, Sucrose, Glycerol, Sodium OrthoVanadate
Buffer N	HEPES (pH 7.9), MgCl2, NaCl, EDTA, Glycerol, Sodium OrthoVanadate
Buffer M	HEPES (pH 7.9), MgCl2, KCl, EDTA, Sucrose, Glycerol, Sodium deoxycholate, NP-40, Sodium OrthoVanadate
Buffer CS	PIPES (pH 6.8), MgCl2, NaCl, EDTA, Sucrose, SDS, Sodium OrthoVanadate

100 mg of decellularized and native tissues (kidney or bladder) were homogenized in 500 µL of Buffer C containing protease inhibitor until the tissues were completely disrupted and a homogeneous suspension was obtained. The homogenate was incubated on a rotator for 20 minutes at 4°C. After incubation, it was centrifuged at 16,000 x g for 20 minutes at 4 °C and the supernatant was discarded. This step was to extract cytosolic proteins. The pellet was washed in 400 µL of Buffer W containing protease inhibitor and the suspension solution was incubated on a rotator for 20

minutes at 4 °C. The suspension solution was centrifuged at 16,000 x g for 20 minutes at 4 °C and the supernatant was discarded. In order to extract nuclear proteins, the pellet was re-suspended in 150 µL of Buffer N containing protease inhibitor, deoxyribonuclease I (DNase I, New England Biolabs, M0303S, MA, USA) and ribonuclease A (RNase A, QIAGEN, 19101, Hilden, Germany). The final concentration of DNase I and RNase A in Buffer N was 200 µg/ml and 20 µg/ml, respectively. The sample was incubated on a rotator for 30 minutes at 4 °C and later on centrifuged at 16,000 x g for 30 minutes at the same temperature. The supernatant obtained was discarded. Furthermore, to extract membrane protein, the pellet was re-suspended in 100 µL of Buffer M containing protease inhibitor and the sample was incubated on a rotator for 30 minutes at 4 °C followed by centrifugation at 16,000 x g for 30 minutes at the same temperature. The supernatant obtained was discarded. Afterward, to extract cytoskeletal proteins, the pellet was re-suspended in 200 µL of Buffer CS containing protease inhibitor and the sample was incubated on a rotator for 30 minutes at room temperature followed by centrifugation at 16,000 x g for 30 minutes also at room temperature. The supernatant obtained from this step was discarded. To perform additional wash of the pellet, it was re-suspended in 500 µL of PBS containing protease inhibitor and the suspension was incubated on a rotator for 5 minutes at 4 °C. Similarly, the suspension was centrifuged at 16,000 x g for 5 minutes at the same temperature. The supernatant obtained was discarded and this wash procedure was repeated for three times. At this point, the pellet remaining was the extraction of insoluble ECM-enriched proteins of the tissue. For further proteomic analyses, these proteins were digested into soluble peptides.

b) In-solution digestion of ECM-enriched proteins

The ECM-enriched pellet was re-suspended in 8 M urea (100 µL) and was agitated at 1,400 rpm for 2 hours at 37 °C. The sample was cooled to room temperature and was added with 2 µL of 500 mM 1, 4-Dithiothreitol (DTT, Sigma-Aldrich, 10197777001, Darmstadt, Germany) to achieve a final concentration of 10 mM. The mixture solution was incubated with continuous agitation at 1,400 rpm for 2 hours at 37 °C. 5 µL of 500 mM iodoacetamide (Thermo Fisher, 90034, MA, USA) was added to prevent the formation of disulfide bonds and ended up with final concentration of 25 mM. The mixture solution was incubated in the dark for 30 minutes at room temperature to complete alkylation. The mixture was then diluted to a 2 M urea concentration with 100 mM ammonium bicarbonate pH 8.0 (Sigma-Aldrich, 09830, Darmstadt, Germany) prepared with ddH2O. Afterward, 4 µL of peptide-N-glycosidase F (2000 U) (PNGase F, New England Biolabs, P0704S, MA, USA) used to remove N-linked oligosaccharides from glycoproteins was added and followed with continuous agitation at 1,400 rpm for 2 hours at 37 °C. In addition, 4 µL of mass spectrometry grade endoproteinase LysC (2 µg) (New England Biolabs, P8109S, MA, USA) was pipetted to the mixture followed with continuous agitation at 1,400 rpm for 2 hours at 37 °C to ensure peptide bonds at the carboxyl side of lysine were cleaved. An aliquot of 10 µL of mass spectrometry grade trypsin (5 µg) (Thermo Fisher, 90057, MA, USA) was added to the mixture and was incubated with continuous agitation at 1,400 rpm overnight at 37 °C, the cloudy solution turned cleared overnight. Another 6 µL (3 µg) of mass spectrometry grade trypsin was added to the mixture followed with continuous agitation at 1,400 rpm for 2 hours at 37 °C. To inactivate the trypsin, the mixture was

acidified with freshly prepared LC-MS grade 50% trifluoroacetic acid (TFA, Thermo Fisher, 85183, MA, USA) pipetted in 1 µL increment (4 µL used in total) until the pH was less than 2.0. Finally, the acidified solution was centrifuged at 20,000 x g for 5 minutes at room temperature and the supernatant was collected. The peptides were desalted by solid phase extraction with C18 Sep-Pak cartridges (Thermo Fisher, 60108, MA, USA) and it was used according to the instructions from the manufacturer and the mixture was eluted with freshly prepared 60% LC-MS grade acetonitrile (ACN) (Sigma-Aldrich, 51101, Darmstadt, Germany) and 0.1% TFA, followed by concentration in a vacuum concentrator (vacuum dried to about 25 µL). Protein concentration was measured spectrophotometrically using NanoDrop technology and peptide solutions were diluted to a final concentration of 0.5 µg/µL with 0.2% formic acid. The samples were stored at -80 °C until LC-MS/MS analysis.

c) Liquid Chromatography-Tandem Mass Spectrometry (LC-MS/MS)

Approximately 1 µg protein digest (in loading buffer made of 5% ACN and 0.1 % TFA) from decellularized and native kidney or bladder tissues were analyzed using an EASY-nLC 1200 chromatography system (Thermo Fisher, LC140, MA, USA) coupled to an Orbitrap Fusion Lumos mass spectrometer (Thermo Fisher, IQLAAEGAAPFADBMBHQ, MA, USA). The EASY-nLC 1200 chromatography system was set up with the acclaim PepMap ESLC C18 LC 75 µm × 50 cm; 3 µm columns (Thermo Fisher,164570, MA, USA) at 50 °C using the following gradient: 0 – 5 minutes 2% ACN; 5-140 minutes, 2 – 28% ACN;140 – 150 minutes,28 – 40% ACN; 150 – 160 minutes, 40 – 95% ACN; 160 – 170 minutes, 95% ACN. The washout step was

performed at a flow rate of 0.5 µL/min at 80% ACN for 12 minutes prior to column equilibration. The total run time was about 3 hours.

A full mass scan (375 – 1500 m/z, 2400V) was performed in the Orbitrap Fusion Lumos mass spectrometer at a resolution of 1,200,00. Data was collected with peptide monoisotopic selection (5 × 104 threshold, charge states 2 – 7, 60-second dynamic exclusion, quad isolation m/z of 0.8). The most intense peaks were selected for fragmentation, and the higher-energy collisional dissociation (HCD) was automatically determined by the instrument based on the m/z values and charged stated of the peptides. The fragmentation spectra were analyzed and the MS raw files were downloaded from the PeptideAtlas data repository. Data was processed using Thermo Proteome Discoverer 2.1 with Sequest and the Rattus norvegicus dataset (SwissProt TaxID=10116, 2017-10-25) with the following parameters: precursor mass 350-5000 Da; enzyme, trypsin; missed cleavage, 2; min/max peptide length 6/144; precursor/fragment tolerance, 10 ppm/0.02 Da; all neutral losses; b,y ions only; static modification, carbamidomethyl; dynamic modifications, oxidation (K, M, P), protein terminus acetyl; Cn max 0.05; PSM, peptide and decoy DB target FDR's, 0.01 strict, 0.05 relaxed, based on q-value. Filtering was set for peptides at least medium confidence. However, only high confidence data was selected with final post process filtering with Proteome Discoverer software (Thermo Scientific, OPTON-30795). Protein and Protein Group were exported to Excel for further sorting and analyses. The full-protein profiling described above is a qualitative analysis to identify existence of different proteins in both native and decellularized tissues. However, it also

indirectly provides quantitative information based on the relative peak intensity and peak width of the individual peptides which means the coverage number could potentially represent relative abundance of each protein. Relative ion intensity was measured by the area under the curve of each peak and was compared to the extracted ion chromatogram standard.

2.5 Recellularization protocols

Decellularized organ-ECMs went through series of evaluation and characterization procedures as described in section 2.3 and 2.4 to ensure their eligibility as starting materials for ECM recellularization. In this study, recellularization is to reseed corresponding human normal or cancerous cells to the decellularized kidney or bladder ECMs. Reseeded cells were expected to proliferate, migrate and even produce their own matrices within the decellularized ECMs (39)**.** However, inconsistencies between different batches of recellularization were observed. Considering the completion/success of recellularization mainly relied on three aspects: **1)** Viability of the cells, **2)** reseeding technique, and **3)** control of cell culture conditions (particularly in close watch of mycoplasma contamination since it is undetectable with just a microscope). The aim of this study was to observe different cells proliferating in a certain location of the ECMs, in other words, to observe similar cell-distribution compare to that observed in a native organ. Nevertheless, any experimental inconsistencies in between would cause failure or inefficiency of

recellularization and ended up with random cell-penetration/adhesion to the ECM, which is to the contrary of the research hypotheses.

2.5.1 Cell lines

Human bladder cancer cell line UM-UC-3 and immortalized epithelial cell line SV-HUC were kindly provided by Dr. Peter Black (Vancouver Prostate Centre, Vancouver, BC, Canada). Human embryonic kidney 293 cell line HEK293 was generously provided by Dr. Amina Zoubeidi (Vancouver Prostate Centre, Vancouver, BC, Canada). Human umbilical vein endothelial cells (HUVEC) were attained from Lonza (CC-2953, Basel, Switzerland). Human dermal fibroblast cells were isolated from neonatal foreskin undergoing circumcision and kindly provided by Dr. Aziz Ghahary. Human metastatic clear cell renal cell carcinoma (ccRCC) cell line (Caki-1) was purchased from American Type Culture Collection (Manassas, Virginia, USA). All media used in this study except EBM ™-Plus was supplemented with 1% Antibiotic-Antimycotic (Gibco, 15240062, ON, Canada) to prevent bacterial and fungal comtamination. Fibroblasts and HEK293 cells were grown in Dulbecco's Modified Eagle Medium (DMEM) (Gibco, 11995-065, ON, Canada) with 10% fetal bovine serum (FBS) (Gibco, 10437028, ON, Canada). SV-HUC were cultured in Keratinocyte Serum-Free Medium (KSFM) (Gibco, 17005042, Carlsbad, CA) supplemented with bovine pituitary extract (50 µg/ml) and recombinant human epidermal growth factor (rhEGF) (0.2 µg/ml). Caki-1 cells were cultured in McCoy's 5A medium (ATCC, 30-2007, Virginia, USA) supplemented with 10% FBS. UM-UC-3 were cultured in Minimal Essential Medium

(MEM) (Gibco,11090-073, ON, Canada) supplemented with 10% FBS, 1% L-glutamine (GlutaMax, 35050061), 1% non-essential amino acids (Gibco, 11140050, Burlington, ON, Canada) and 1% sodium pyruvate (Gibco, 11360070, Burlington, ON, Canada). Reagents used for UM-UC-3 were obtained from Thermo Fisher Scientific (Gibco), Burlington, ON, Canada. HUVEC cells were cultured in Endothelial Cell Growth Basal Medium-Plus (EBM ™-Plus) (Lonza, CC-5036, Basel, Switzerland) supplemented with 2% FBS, 0.1% hydrocortisone, 5% L-glutamine, 0.1% ascorbic acid, 0.1% Heparin, 0.2% Endothelial Growth Supplement (EnGS), 0.1% rhEGF and 0.1% Gentamicin Sulfate-Amphotericin (GA-1000) (Lonza, CC-4542, Basel, Switzerland). All cells used were cultured at 37 °C in a 5% CO_2 incubator and mycoplasma contamination was tested at regular intervals for each cell-line/primary cell. When cells were confluent they were passaged by incubation at 37 °C for 3 - 4 minutes with 0.25% trypsin (Gibco, 25200056, ON, Canada), centrifuged at 1,500 RPM for 5 minutes and resuspension in medium. Cells were stored long term in Bambanker (NIPPON Genetics, BB01, Düren, Germany) at a concentration of one million cells per mL and in liquid nitrogen.

2.5.2 Kidney ECM recellularization protocol

Decellularized kidneys were cut into thin pieces with sterile blades, washed with repeated agitation in 10% Antibiotic-Antimycotic and placed in a 24-well plate (well diameter: 15.6 mm; Well volume: 3.4 mL) (Corning, CL-S3524, ME, USA) with sterile forceps. Tissues were cultured in a mixture of different growth media (for 24 hours)

depending on the different cell types the tissue would be recellularized with. Afterward, all cultured cells were dissociated into single cells using 0.25% trypsin for 4 minutes at 37 °C and centrifuged at 1500 rpm for 5 minutes. Cell pellets were re-suspended with Matrigel Matrix (Corning, 354234, ME, USA) (4,000 cells in 10 µL of Matrigel Matrix). Each 10 µL of the cell-Matrigel mixture were loaded onto the tissue surface. The 24-well plate were incubated in 37 °C with 5% CO_2 for 2 hours to ensure the mixture loaded were completely solidified while cells could maintain their viability. Tissues were again immersed with corresponding growth media (1 mL of each well) after incubation and the cell-loading steps were repeated 4 – 5 times (from day 10) until reached 21 days of incubation at 37°C. Within the 21-day timespan, media were replaced on a daily basis. At day 21, the recellularized tissues would be fixed in 10% formalin for H&E and immunohistochemistry (IHC) evaluations.

Other earlier tested protocols can be found in appendix D.

2.5.3 Bladder ECM recellularization protocol.

Decellularized bladders were cut approximately into 1 cm × 1 cm × 0.5 cm pieces and placed in a 6-well plate (well diameter: 34.8 mm; Well volume: 16.8 mL) (Corning, CL-S3516, ME, USA). Tissue was placed on cell culture inserts (Fisher Scientific, 08-771, PA, USA) using sterile forceps and the orientation of the bladder's placement was crucial in this study. After decellularization, the bladder matrix clearly shows two sides, one surface is visibly shiny (Adventitia) and the other gives the appearance of a rough

surface (Lumen side). Starting at the lumen and moving outward through the bladder wall, the urothelium (mucosa) consists of three layers: umbrella cells, intermediate cells and basal cells. The lamina propria (basement membrane) underlies the basal cells and separates the urothelium from stromal cells layer (submucosa) and muscles. In this study, muscularis propria of the bladder was removed to some extent in order to expose stroma for recellularization of fibroblasts and HUVECs while SV-HUC and UM-UC-3 were recellularized on the urothelium.

For either single cell-type or multi cell-type recellularization, bladder tissues were immersed in different growth media according to cell types being reseeded. Tissues for single cell-type recellularization: HUVECs were with EBM ™-Plus, fibroblasts were with DMEM supplemented with 10% FBS, SV-HUCs were cultured with KSFM kit and UM-UC-3 were with MEM supplemented with 10% FBS, 1% L-glutamine, 1% non-essential amino acids and 1% sodium pyruvate. Bladders recellularized with HUVEC: fibroblast: SV-HUC (ratio of 2: 1: 2) required a combination of all corresponding media described above at 1:1:1 ratio. Prior to recellularization of the aforementioned cells, decellularized ECMs were immersed in media with corresponding growth factor for 24 hours. Cells grown in 2D culture were trypsinized and counted. For single cell type recellularization, cell concentration of 2×10^6 cells/cm^3 was applied. For multi cell-type recellularization, cell concentration of 2×10^6 cells/cm^3 (HUVEC, SV-HUC, respectively) was reseeded while 1×10^6 cells/cm^3 of fibroblasts was reseeded. All cells were dissociated into single cells using 0.25% trypsin for 4 minutes at 37 °C and centrifuged at 1,500 rpm for 5 minutes. Each cell types were re-suspended with

Matrigel Matrix (1×10^6 cells in 50 µL of Matrigel Matrix). Each 50 µL of the cell-Matrigel mixture were loaded onto the tissue surface. For multi cell-type recellularization, bladder tissues were flipped in order to load cells into their corresponding environment (SV-HUC and UM-UC-3 on urothelium; fibroblast and HUVEC on the stromal layer). The 6-well plate were incubated in 37 °C with 5% CO2 for 2 hours to ensure the mixture loaded were completely solidified while cells could maintain their viability. Tissues were then immersed with corresponding growth media (3 mL of each well) after incubation and the cell-loading step were repeated with 4 – 5 times (from day 10) until reached 21 days of incubation at 37 °C. Within the 21-day timespan, media were replaced on a daily basis. Disturbing of the tissues during incubation was minimized. At day 21, the recellularized tissues were fixed in 10% formalin for H&E and IHC evaluations.

Other earlier tested protocols can be found in appendix E & F.

2.6 Evaluation of recellularization protocols

a) IHC

To evaluate cells' position, distribution and penetration after being reseeded, both kidney and bladder tissues were fixed in 10% formalin for 24 hours followed by immersing in 70% prior to H&E. H&E was performed as described in section 2.3.2 (a). For single cell-type recellularization of kidney and bladder, H&E only was sufficient for the evaluating purposes. However, for bladder multi cell-type recellularization, IHC

staining would be essential to identify cell types and their distributions. Formalin-fixed, paraffin-embedded tissue sections were prepared as described in section 2.3.2 (a) and before proceeding to IHC staining, the section slides were deparaffinized and rehydrated. The slides were placed in a rack and were immersed in 100% xylene for 10 minutes; this step was repeated for three times. The slides were then immersed in 100% ethanol for 5 minutes and this step was repeated for two times. Next, the slides were immersed in 95% for 5 minutes and this step was repeated for two times followed by immersion in 80% and 70% ethanol for 5 minutes, respectively. After rehydration, the slides were rinsed with tap water until ready to perform antigen retrieval. Antigen retrieval was performed by boiling the slides (850W, microwave) in Tris/EDTA (pH 9.0) for 10 minutes followed with immersion in the Antigen Unmasking Solution (1:1 with H_2O) (Vector Laboratory, H-3301, CA, USA). The slides were cooled down to room temperature on ice and then rinsed briefly with dH_2O and PBS. Endogenous peroxidase was blocked by 0.3% H_2O_2 in tris-buffer saline (TBS) for 10 minutes and then rinsed with PBS for 5 minutes, three times in total. Non-specific binding sites were blocked by 4% goat serum (Abcam, ab7481, ON, Canada) in PBS and left in room temperature for 1 hour. Afterward, the slides were incubated with pre-diluted Anti-CD31 antibody (specifically react with human CD31) (Abcam, ab76533, ON, Canada) and pre-diluted Anti-Vimentin antibody (specifically react with human vimentin) (Abcam, ab16700, ON, Canada) overnight at 4 °C. After incubation, the slides were rinsed in PSB with agitating three times for 15 minutes. The slides were then incubated with streptavidin HRP (horseradish peroxidase) at 37 °C for 30 minutes (Abcam, ab7403, ON, Canada) followed by PBS rinsing, five times for 5 minutes.

Finally, the slides were incubated with 3,3'- diaminobenzidine (DAB) (Abcam, ab64238, ON, Canada) for 5 minutes at room temperature. After rinsing with running water, the slides were counterstained in Mayer's hematoxylin solution (Sigma Aldrich, MHS1, Darmstadt, Germany), dehydrated and mounted prior to cover-slipped visualization. The slides were then scanned with Leica SCN400 slide scanner (Meyer Instruments).

b) Penetration rate of fibroblasts

Fibroblasts reseeded to the bladder tissues were expected to penetrate and eventually randomly distributed in the lamina propria due to its cell-nature (40). In this study, we calculated fibroblasts' penetration rate into the decellularized ECM (distance vs. time). The penetration distance was measured from the H&E slide (tissue cross section) using digital ruler; multiple measurements were applied from the surface of stroma to the location where the cells were visualized. Mean distance was then calculated based on these measurements. In this case, with the tissue's thickness being measured, the penetration rate of fibroblasts was calculated based on a 21-day timespan. Student's t-test was performed to ensure the statistical significance of this calculation.

Chapter 3: Results

3.1 Optimized kidney decellularization protocol

Kidneys, obtained from rodents, were decellularized by perfusion through the abdominal aorta using the protocol described in chapter 2. This process led to an almost translucent appearance with gross preservation of ECM microarchitecture upon visual inspection (Figure 5-D). In this study, the completeness of decellularization is confirmed when there are no visible nuclear materials in histological assessment with H&E, and less than 5% residual DNA content or less than 50 nanogram of double-stranded DNA per milligram dry weight (37). These criteria are widely accepted for organ decellularization based on previous endpoint analysis by destructive methods (41). Other attempts using different protocols described in the appendix section did not completely decellularize the organs and caused significant damage to the ECM.

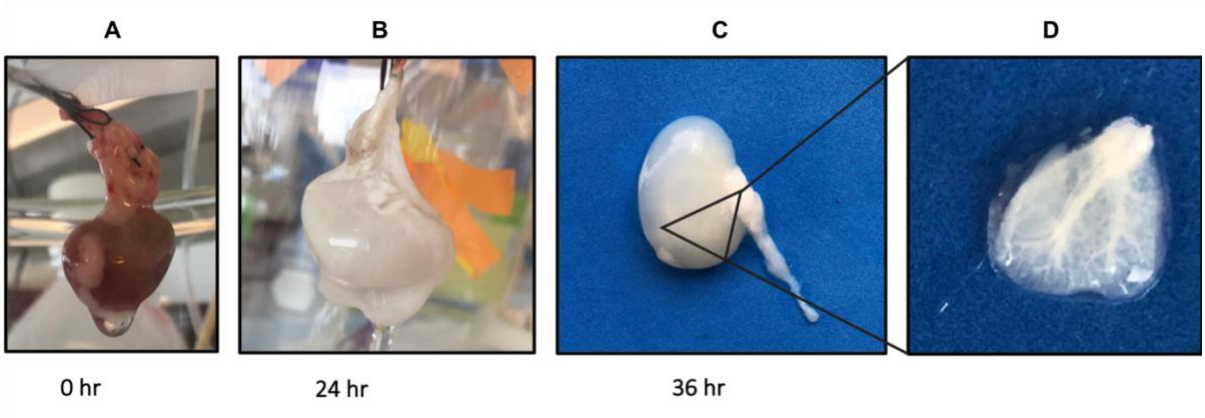

Figure 5. Macroscopic assessment of native (A) and decellularized (B, C, D) kidney. (A) The native kidney under decellularization at timepoint 0. **(B)** The same kidney under decellularization after 24 hours. **(C)** The same kidney completed decellularization after 36 hours. **(D)** A piece of decellularized kidney from **(C).**

3.1.1 Residual DNA quantification of decellularized kidney proved complete cell removal

To evaluate cellular contents within the ECMs, the residual DNA content in both native and decellularized kidney was measured spectrophotometrically using NanoDrop technology. The level of residual DNA in native kidney was compared to those of decellularized ones (110.10 ng/μl ± 4.87 ng/μl; n=5 vs. 4.92 ng/μl ± 0.30 ng/μl SD; n=5. *p*=0.0049) (Figure 6). The measurement of residual DNA in native and decellularized kidneys was repeated for five times, respectively (native kidney: 113.8 ng/μl, 113.2 ng/μl, 113.1 ng/μl, 107.9 ng/μl and 102.5 ng/μl; decellularized kidney: 4.91 ng/μl, 4.59 ng/μl, 4.68 ng/μl, 5.12 ng/μl and 5.30 ng/μl). Statistical analysis was performed using the unpaired (Two Sample) t test. H_0: the DNA concentration of decellularized kidneys equals to 5% of native kidneys' DNA concentration. H_α: the

DNA concentration of decellularized kidneys is less than 5% of native kidneys' DNA concentration. $p<0.05$ rejected the null hypothesis and approved the alternative hypothesis that DNA concentration of decellularized kidneys is less than 5% of native kidneys' DNA concentration with decellularization protocols developed in this study.

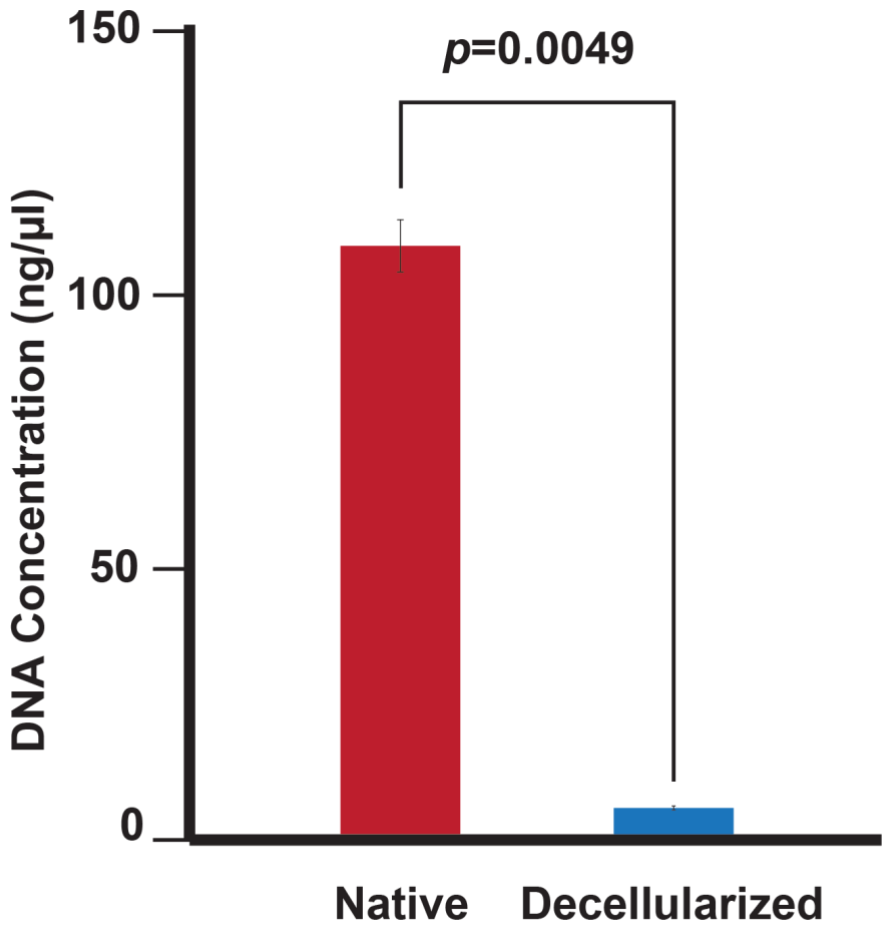

Figure 6. DNA Quantification of native and decellularized kidneys.
Native kidneys have mean DNA concentration of 110.10 ng/µL ± 4.87 ng/µL; n=5 and decellularized kidneys have mean DNA concentration of 4.92 ng/µL ± 0.30 ng/µL; n=5. Statistical analysis was performed using the unpaired (Two Sample) t test, p=0.0049. Data obtained from the R platform.

3.1.2 Evaluation of decellularized kidney reveals complete cell removal and preservation of ECM microarchitectures

Microscopic assessment by H&E staining (in various renal regions) of decellularized kidney mirrored the macroscopic evaluation that gross preservation of ECM microarchitecture was achieved (Figure 7). The almost translucent appearance (Figure 7 - B) was suggestive of complete cell removal, which was confirmed by H&E. Panel C, E and G showed medulla, artery and glomerulus of a native kidney that is occupied with cells while panel D, F and H showed there are no cells observed in that of decellularized kidney.

This protocol confirms the preservation of the ECM microarchitecture including delicate structural/functional components such as the glomerulus. They were well preserved and similar in appearance to the native kidney as observed with the SEM. The glomerular tubules in the decellularized kidney coiled less tightly than in that of the native kidney (Figure 8, panel C & D), which, could possibly be caused by the complete loss of cellular components during decellularization. A honeycomb-like appearance of renal medulla was well preserved after decellularization and cells were completely removed compared to that of native kidney (Figure 8, panel A & B). Individual tubules in a glomerulus were visualized at 20X magnifications for native and decellularized kidney (Figure 8, panel E & F). It proved complete cell removal from the glomerulus after decellularization and the preservation of glomerular basement membrane's microarchitecture.

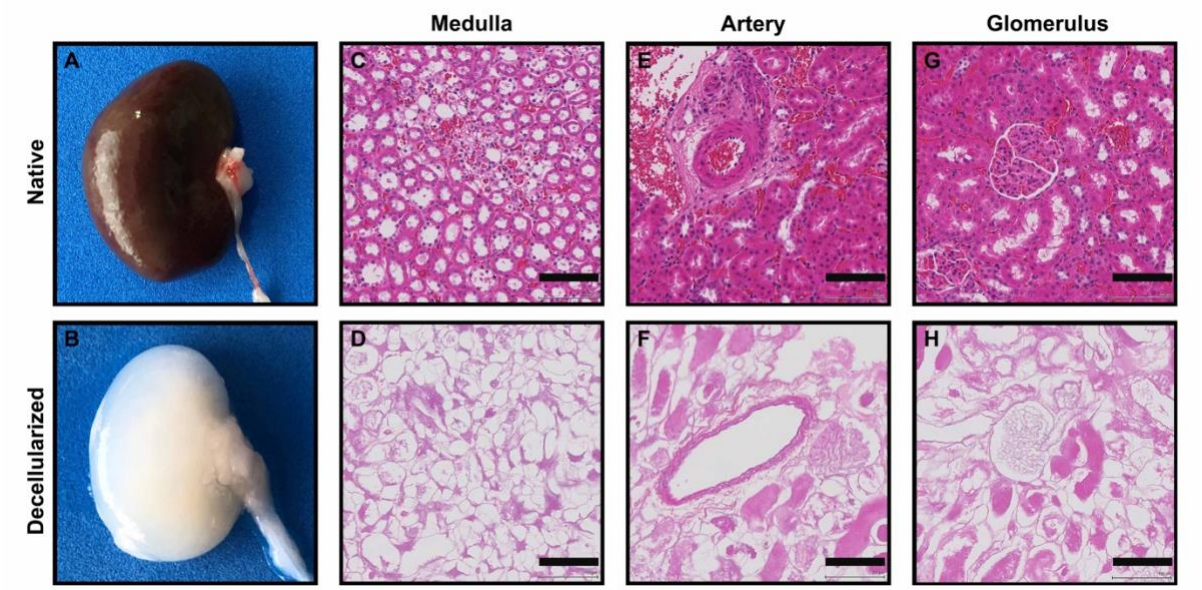

Figure 7. Macroscopic visualization and histological examination of native (A, C, E, G) and decellularized (B, D, F, H) kidney. (A) The entire native kidney with ureter. **(B)** The entire decellularized kidney with ureter. **(C, D, E, F, G, H)** Hematoxylin & Eosin stains (20X): renal medulla of native **(C)** and decellularized **(D)** kidney. Renal artery of native **(E)** and decellularized **(F)** kidney. Glomerulus of native **(G)** and decellularized **(H)** kidney.
Scale bars in panel C, D, E, F, G and H represent 100 μm.

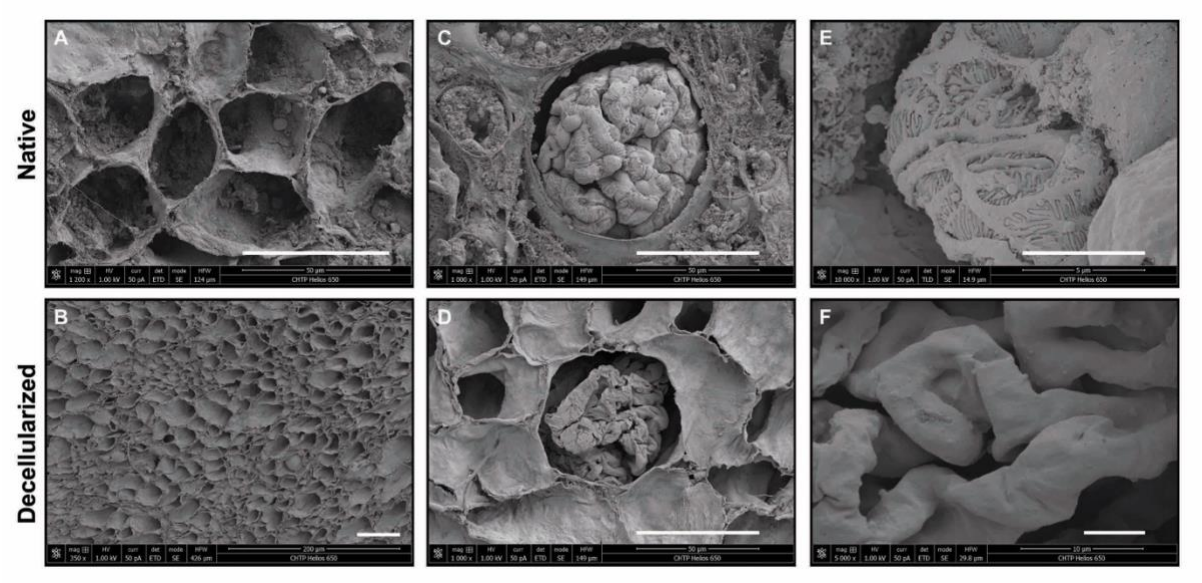

Figure 8. Structural analysis of native (A, C, E) and decellularized (B, D, F) kidneys. SEM images: **(A)** Renal medulla of native kidney (1200X). Cells are observed inside of the renal medulla. **(B)** Renal medulla of decellularized kidney (350 X). No cells are observed. **(C)** Glomerulus of native kidney (1000X). Cells are observed in the tubules next to the glomerulus. **(D)** Glomerulus of decellularized kidney (1000X). No cells are observed and the structure of the glomerulus is preserved. **(E)** Glomerular basement membrane & epithelial podocytes of native kidney (10,000X). Cells are clearly showed on the tubule. **(F)** Glomerular basement membrane of decellularized kidney (5000X), epithelial podocytes were unseen.
Scale bars in panel A, B, C and D represent 50 μm; scale bars in panel E and F represent 5 μm.

3.1.3 Structural protein and ECM-bound growth factors are preserved after decellularization of kidney.

Once kidneys were decellularized and the remaining DNA concentration was less than 5% compare to that of native tissue, I wanted to evaluate the remaining full-protein profile of the decellularize kidney ECM. Both native and decellularized kidneys were evaluated using LC-MS/MS (Table 1 and 2). The most abundant components of the rodent kidney ECM are collagen IV and laminin which are important to the formation of glomerular basement membrane that supports tubule formation and renal development (42) (43) (44)**.** Structural proteins such as collagen IV and laminin were preserved with the optimized decellularization protocol. Synthesized by glomerular cells, fibronectin is a major structural and functional component of the ECM that plays important roles in cell adhesion, growth, migration and differentiation (45). Proteins that interact or bind to fibronectin such as decorin, biglycan and gelsolin that are crucial in matrix assembly (46) (47) (48) was also preserved after decellularization. Another type of structural proteins in the ECM preserved are fubulins. They associate with basement membrane and elastic fibers and interact with many extracellular matrix constituents including fibronectin and laminins (49). Other functional proteins such as galectin, which has broad functions including mediation of cell-cell interaction, cell-matrix adhesion and transmembrane signaling in the ECM (50) were seen in both native and decellularized kidneys. Therefore, the existence of galectin may ensure the recellularization potency in future experiments. Overall, proteins that play key roles in maintaining ECM functionality were preserved after decellularization.

Growth factors such as Transforming growth factor is responsible in epithelial cell differentiation (51)**.** The existence of this growth factor was indirectly proved by finding the protein it secreted (Transforming growth factor beta-1 induced transcript 1 protein) in both native and decellularized kidneys under the optimized decellularization protocol developed in this study.

Table 1. Proteomic analysis of decellularized (Rattus norvegicus) kidney

Accession	Decellularized Kidney Protein	Coverage	Number of Peptides	Number of Unique peptides	MW [kDa]
Q4FZU4	ADAMTS-like protein 4	1.941747573	2	2	112.7
O35889-1	Afadin	1.202843084	2	2	207.5
P47853	Biglycan	38.21138211	10	9	41.7
P47854	Cathepsin B	7.374631268	2	2	37.4
P47855	Ceruloplasmin	6.987724268	7	7	120.8
P47856	Clusterin	25.05592841	10	10	51.3
P47857	Collagen alpha-1(I) chain	64.34962147	93	90	137.9
P47858	Collagen alpha-1(II) chain	20.71881607	20	18	134.5
P47859	Collagen alpha-1(III) chain	50.10252905	82	80	138.9
P47860	Collagen alpha-1(V) chain	14.07608696	21	17	183.9
P47861	Collagen alpha-1(XI) chain	10.75388027	16	13	180.9
P47862	Collagen alpha-1(XII) chain	18.92744479	5	5	32
P47863	Collagen alpha-2(I) chain	66.39941691	81	81	129.5
P47864	Decorin	16.10169492	6	5	39.8
P47865	Dystrobrevin beta	3.669724771	3	3	73.8
P47866	Dystrophin	1.087843351	5	3	425.6
P47867	Elastin	6.551724138	2	2	73.3
P47868	Extracellular matrix protein 1	10.3202847	6	6	63.2
P47869	Fibrinogen alpha chain	21.35549872	16	16	86.6
P47870	Fibrinogen beta chain	43.42379958	18	18	54.2
P47871	Fibrinogen gamma chain	36.85393258	19	19	50.6
P47872	Fibronectin	29.10779168	55	55	272.3
P47873	Fibulin-5	19.41964286	7	7	50.1
P47874	Fibulin-1	6.268656716	2	2	36.6
P47875	Galectin-1	34.07407407	4	4	14.8
P47876	Gelsolin	15.12820513	10	10	86
P47877	Isoform 2 of Alpha-1B-glycoprotein	3.382663848	2	2	112.7
P47878	Isoform 2 of Collagen alpha-1(XI) chain	10.68281938	16	13	207.5
P47879	Isoform 2 of Elastin	6.909090909	2	2	41.7
P47880	Isoform 2 of Fibrinogen alpha chain	30.36363636	16	16	37.4
P47881	Isoform 2 of Fibrinogen beta chain	39.76143141	17	17	120.8
P47882	Isoform 2 of Fibronectin	29.66066192	54	54	51.3
P47883	Isoform 2 of Gelsolin	16.14227086	10	10	137.9
P47884	Isoform 2 of Nidogen-2	53.97727273	11	11	134.5
P47885	Isoform 3 of Collagen alpha-1(XI) chain	10.99150142	16	13	138.9
P47886	Isoform 3 of Elastin	6.559263521	2	2	183.9

Accession	Decellularized Kidney Protein	Coverage	Number of Peptides	Number of Unique peptides	MW [kDa]
P47888	Isoform 4 of Collagen alpha-1(XI) chain	11.28563118	16	13	32
P47889	Isoform 4 of Elastin	6.666666667	2	2	129.5
P47890	Isoform 4 of Fibronectin	30.57675997	55	55	39.8
P47891	Isoform 5 of Collagen alpha-1(XI) chain	11.20739457	16	13	73.8
P47892	Isoform 5 of Elastin	6.917475728	2	2	425.6
P47893	Isoform 6 of Collagen alpha-1(XI) chain	11.54761905	16	13	73.3
P47894	Isoform 6 of Elastin	6.674473068	2	2	63.2
P47895	Isoform 7 of Elastin	7.037037037	2	2	86.6
P47896	Isoform 8 of Elastin	7.045735476	2	2	54.2
P47897	Isoform Gamma-A of Fibrinogen gamma chain	37.52860412	19	19	50.6
P47898	Isoform Short of Collagen alpha-1(XII) chain	22.90076336	93	5	272.3
P47899	Laminin subunit beta-2	59.68906163	8	93	50.1
P47900	Lumican	26.33136095	7	8	36.6
P47901	Metalloproteinase inhibitor 3	31.27962085	3	7	14.8
P47902	Nidogen-1	8.333333333	35	3	86
P47903	Nidogen-2	33.5243553	4	35	52.5
P47904	Plasminogen	7.266009852	2	4	182.1
P47905	Syntenin-1	7	2	2	112.7
P47906	Uromodulin	2.639751553	5	16	207.5
P47907	EGF-containing fibulin-like extracellular matrix protein 1	16.02434077	5	17	41.7
P47908	Hepatocyte growth factor-regulated tyrosine kinase substrate	5.154639175	5	54	37.4
P47909	Isoform 2 of Hepatocyte growth factor-regulated tyrosine kinase substrate	5.188067445	9	10	120.8
P47910	Latent-transforming growth factor beta-binding protein 1	6.83411215	6	11	51.3
P47911	Transforming growth factor beta-1-induced transcript 1 protein	15.18438178	6	13	137.9

Table 2. Proteomic analysis of native (Rattus norvegicus) kidney

Accession	Native Kidney Protein	Coverage	Number of Peptides	Number of Unique peptides	MW [kDa]
A2RUV9	Adipocyte enhancer-binding protein 1	8.333333333	6	6	128
O35889-1	Afadin	3.280481137	5	5	207.5
P36953	Afamin	3.125	2	2	69.3
P25304-1	Agrin	12.86370597	18	18	208.5
P14046	Alpha-1-inhibitor 3	22.74881517	29	9	163.7
Q63041	Alpha-1-macroglobulin	38	46	46	167
P24090	Alpha-2-HS-glycoprotein	43.18181818	10	10	38
P01015	Angiotensinogen	22.43186583	8	8	51.9
P04639	Apolipoprotein A-I	16.21621622	5	5	30
P02651	Apolipoprotein A-IV	38.87468031	12	12	44.4
Q7TMA5	apolipoprotein B-100	12.14421252	43	43	535.7
Q9ESS6	Basal cell adhesion molecule	21.79487179	10	10	67.5
P26644	Beta-2-glycoprotein 1	29.96632997	9	9	33.2
P47853	biglycan	24.66124661	6	5	41.7
Q63514	C4b-binding protein alpha chain	19.35483871	10	9	62.2
P00787	Cathepsin B	36.87315634	11	11	37.4
P24268	Cathepsin D	21.62162162	6	6	44.7
P07154	Cathepsin L1	14.97005988	4	4	37.6
P13635	Ceruloplasmin	5.571293673	4	4	120.8
Q00657	Chondroitin sulfate proteoglycan 4	1.891659501	3	3	251.8
P05371	Clusterin	16.55480984	6	6	51.3
P02454	Collagen alpha-1(I) chain	48.7267722	54	53	137.9
P05539	Collagen alpha-1(II) chain	3.03030303	3	1	134.5
P13941	Collagen alpha-1(III) chain	33.15105947	42	41	138.9
Q9JI03	Collagen alpha-1(V) chain	3.532608696	4	3	183.9
P20909-1	Collagen alpha-1(XI) chain	1.884700665	3	2	180.9
P70560-1	Collagen alpha-1(XII) chain	7.255520505	2	2	32
P02466	Collagen alpha-2(I) chain	45.40816327	44	44	129.5
P31720	Complement C1q subcomponent subunit A	10.20408163	2	2	25.9
P01026	Complement C3	34.69633193	48	48	186.3
P08649	Complement C4	18.88313184	25	25	192
O35796	Complement component 1 Q subcomponent-binding protein, mitochondrial	26.52329749	4	4	31
Q811M5	Complement component c6	5.139186296	3	3	105
P55314	Complement component C8 beta chain	3.904923599	2	2	66.6
Q62930	complement component C9	28.33935018	15	15	62.2
Q63135-1	Complement component receptor 1-like protein	10.19677996	4	4	61.6

Accession	Native Kidney Protein	Coverage	Number of Peptides	Number of Unique peptides	MW [kDa]
Q9WUW3	Complement factor I	7.450331126	3	3	67.3
P31211	corticosteroid-binding globulin	7.828282828	3	3	44.6
Q01129	decorin	15.53672316	6	5	39.8
Q7M0E3	Destrin	60.60606061	13	12	18.5
Q9QX79	Fetuin-B	38.88888889	9	9	41.5
P06399	Fibrinogen alpha chain	34.65473146	23	23	86.6
P14480	Fibrinogen beta chain	65.55323591	32	32	54.2
P02680-1	Fibrinogen gamma chain	58.20224719	26	26	50.6
P04937-1	fibronectin	27.89664917	44	44	272.3
Q9WVH8	Fibulin-5	8.705357143	4	4	50.1
Q9WUH4	Four and a half LIM domains protein 1	26.42857143	6	6	31.9
O35115	Four and a half LIM domains protein 2	60.93189964	14	14	32.1
P11762	Galectin-1	46.66666667	6	6	14.8
P08699	Galectin-3	14.1221374	4	4	27.2
Q68FP1	Gelsolin	40.12820513	23	23	86
P23785	Granulins	5.102040816	2	2	63.3
P06866-1	Haptoglobin	15.56195965	5	5	38.5
P20059	Hemopexin	15.65217391	5	5	51.3
Q64268	Heparin cofactor 2	6.054279749	2	2	54.5
P63159	High mobility group protein B1	30.69767442	7	7	24.9
Q5XIE8	Integral membrane protein 2B	21.42857143	4	4	30.3
P20909-2	Isoform 2 of Collagen alpha-1(XI) chain	1.872246696	3	2	182.1
P06399-2	Isoform 2 of Fibrinogen alpha chain	45.45454545	22	22	60.5
P14480-2	Isoform 2 of Fibrinogen beta chain	59.44333996	30	30	56.6
P04937-2	Isoform 2 of Fibronectin	28.94847088	44	44	262.6
Q68FP1-2	Isoform 2 of Gelsolin	40.35567715	22	22	80.9
P06866-2	Isoform 2 of Haptoglobin	14.17322835	5	5	42.4
Q03626-2	Isoform 2 of Murinoglobulin-1	22.88993923	29	9	164.5
B5DFC9-2	Isoform 2 of Nidogen-2	28.40909091	5	5	20.1
P12346-2	Isoform 2 of Serotransferrin	16.33064516	7	7	54.5
P20909-3	Isoform 3 of Collagen alpha-1(XI) chain	1.926345609	3	2	176.4
P04937-3	Isoform 3 of Fibronectin	28.18107667	44	44	269.6
P20909-4	Isoform 4 of Collagen alpha-1(XI) chain	1.977894124	3	2	171.3
P04937-4	Isoform 4 of Fibronectin	29.30449534	44	44	259.2
P20909-5	Isoform 5 of Collagen alpha-1(XI) chain	1.964182553	3	2	172.5
P20909-6	Isoform 6 of Collagen alpha-1(XI) chain	2.023809524	3	2	166.7
P02680-2	Isoform Gamma-A of Fibrinogen gamma chain	59.26773455	26	26	49.6
P08934-2	Isoform LMW of Kininogen-1	14.54965358	6	3	47.9

Accession	Native Kidney Protein	Coverage	Number of Peptides	Number of Unique peptides	MW [kDa]
P70560-2	Isoform Short of Collagen alpha-1(XII) chain	8.778625954	2	2	25.4
Q9ERB4-2	Isoform V3 of Versican core protein	6.41221374	4	4	74.4
Q9ERB4-3	Isoform Vint of Versican core protein	0.848082596	2	2	296.7
P08934-1	kininogen-1	9.85915493	6	3	70.9
P15800	laminin subunit beta-2	15.32481954	23	23	196.3
P51886	Lumican	32.24852071	10	10	38.3
P30904	Macrophage Migration inhibitory factor	38.26086957	4	4	12.5
P02761	Major urinary protein	62.98342541	12	12	20.7
P48032	Metalloproteinase inhibitor 3	19.43127962	4	4	24.2
Q03626-1	Murinoglobulin-1	22.79757902	29	9	165.2
Q6IE52	Murinoglobulin-2	16.98895028	20	0	161.5
B5DFC9	Nidogen-2	13.18051576	13	13	152.9
Q66H86	Olfactomedin-like protein 1	4.975124378	2	2	45.6
B0BNI5	Olfactomedin-like protein 3	5.911330049	2	2	45.9
P14272	Plasma kallikrein	7.993730408	5	5	71.2
Q6P734	Plasma protease C1 inhibitor	5.158730159	2	2	55.6
Q01177	Plasminogen	49.87684729	30	30	90.5
Q9EQP5	prolargin	21.48541114	6	6	43.2
Q64240	Protein AMBP	28.93982808	9	9	38.8
P18292	Prothrombin	32.90113452	15	15	70.4
P08424	Renin	6.965174129	2	2	44.2
P25236	Selenoprotein P	5.194805195	2	2	43.1
P12346-1	Serotransferrin	16.04584527	10	10	76.3
P02770	Serum albumin	27.63157895	16	16	68.7
P35446	Spondin-1	13.25898389	7	7	90.7
P01048	T-kininogen 1	19.06976744	6	3	47.7
P08932	T-kininogen 2	19.53488372	7	1	47.7
P31232	transgelin	48.25870647	10	10	22.6
Q5XFX0	Transgelin-2	58.79396985	13	13	22.4
P02767	Transthyretin	21.76870748	3	3	15.7
P27590	uromodulin	18.01242236	10	10	71
Q9ERB4	Versican core protein	1.533966399	4	4	299.8
P04276	vitamin D-binding protein	16.80672269	8	8	53.5
P62994-1	Growth factor receptor-bound protein 2	19.35483871	4	4	25.2
Q9JJ50	Hepatocyte growth factor-regulated tyrosine kinase substrate	11.21134021	6	6	86.2
Q8VHK7	hepatoma-derived growth factor	19.83122363	5	5	26.5
P62994-2	Isoform 2 of Growth factor receptor-bound protein 2	20.68965517	4	4	23.5

Accession	Native Kidney Protein	Coverage	Number of Peptides	Number of Unique peptides	MW [kDa]
Q9JJ50-2	Isoform 2 of Hepatocyte growth factor-regulated tyrosine kinase substrate	11.28404669	6	6	85.7
P62994-3	Isoform 3 of Growth factor receptor-bound protein 2	37.28813559	2	2	6.9
Q6P686	osteoclast-stimulating factor 1	25.70093458	4	4	23.7
Q99PD6	Transforming growth factor beta-1-induced transcript 1 protein	10.62906725	4	4	50.1

3.2 Optimized bladder decellularization protocol.

Pig bladders were harvested and opened through a mid-line incision to form a flat butterfly-like shape. Once the epithelium is exposed, the bladder is sectioned into multiple 1 cm × 1 cm × 0.5 cm squares (Figure 10 - A) and decellularized by immersion using the protocol described in section 2.2.4 (Figure 10 - B). After decellularization, the bladders started to show clear white color with contracted appearances. It was proved in this study that immersion decellularization can be completed in fewer cycles with increased centrifugal forces (larger petri dishes used). Other attempts using different protocols described in the appendix section did not achieve complete decellularization since the tissues failed to show homogenous clear white appearance.

3.2.1 Residual DNA quantification of decellularized bladder proved complete cell removal

To evaluate cell removal using our protocol, the residual DNA content in both native and decellularized bladder ECM was measured spectrophotometrically using NanoDrop technology. The level of residual DNA in native bladders was compared to those of decellularized bladders (55.9 ng/μl ± 3.41 ng/μl; n=5 vs. 2.61 ng/μl ± 0.42 ng/μl; n=5. p=0.013) (Figure 9). The measurements of residual DNA in native and decellularized bladder were repeated for five times, respectively (native bladders: 60.4 ng/μl, 54.3 ng/μl, 51.3 ng/μl, 57.4 ng/μl and 55.8 ng/μl; decellularized bladders: 2.79

ng/μl,1.96 ng/μl, 2.41 ng/μl, 3.01 ng/μl and 2.87 ng/μl). Statistical analysis was performed using the unpaired (Two Sample) t test. H_0: the DNA concentration of decellularized bladders equals to 5% of native bladders' DNA concentration. H_α: the DNA concentration of decellularized bladders is less than 5% of native bladders' DNA concentration. $p<0.05$ rejected the null hypothesis and approved the alternative hypothesis that DNA concentration of decellularized bladders is less than 5% of native bladders' DNA concentration.

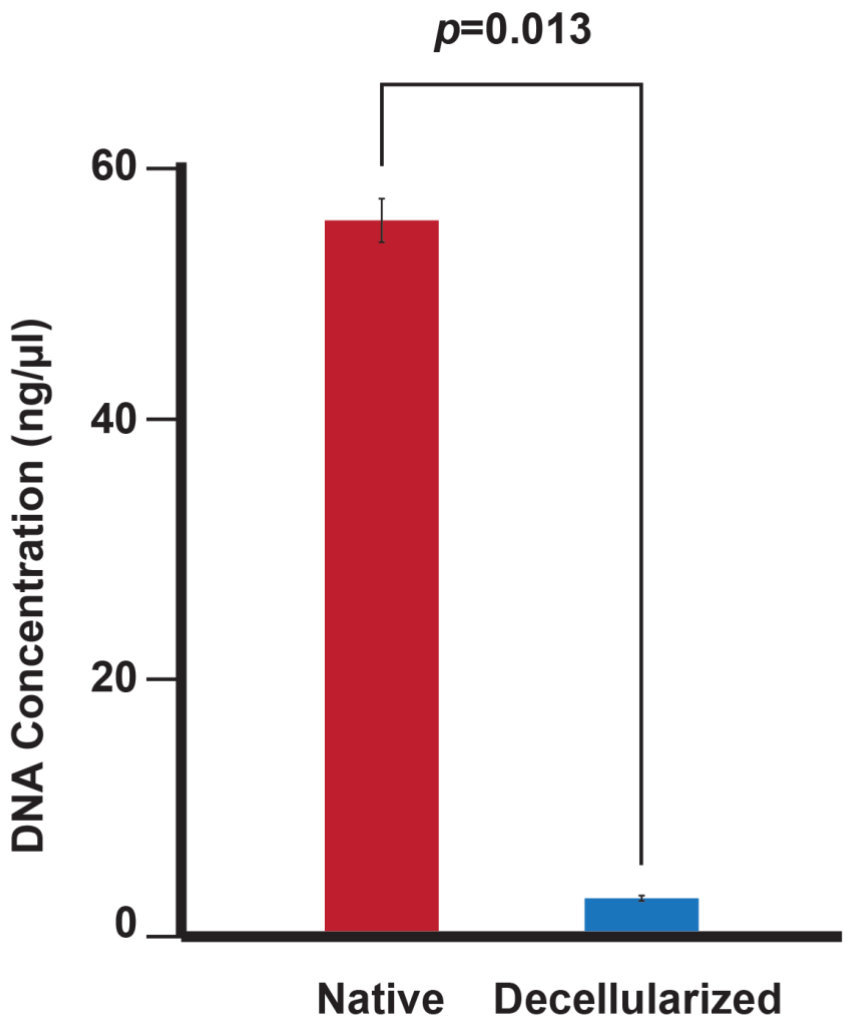

Figure 9. DNA Quantification of native and decellularized bladders.
Native bladders have mean DNA concentration of 55.9 ng/µL ± 3.41 ng/µL n=5 and decellularized bladders have mean DNA concentration of 2.61 ng/µL ± 0.42 ng/µL; n=5. Statistical analysis was performed using the unpaired (Two Sample) t test, *p*=0.013. Data obtained from the R platform.

3.2.2 Evaluation of decellularized bladder reveals complete cell removal and preservation of ECM microarchitectures

H&E stains of decellularized bladders (4X and 20X magnification) illustrated that the urothelial and stromal cells were completely removed after decellularization as compared to those of native tissues (Figure 10, panel E & F) and the clear border between stroma and muscle layer was observed (Figure 10, panel C & D). The ECM microarchitecture was further evaluated using SEM. Panel B and D from Figure 11, show a surface image of the basement membrane of the decellularized bladder showing no cells left from the urothelium. Panel A and C clearly show the hexagonal cells characteristic of the umbrella cells from the urothelium in a native bladder.

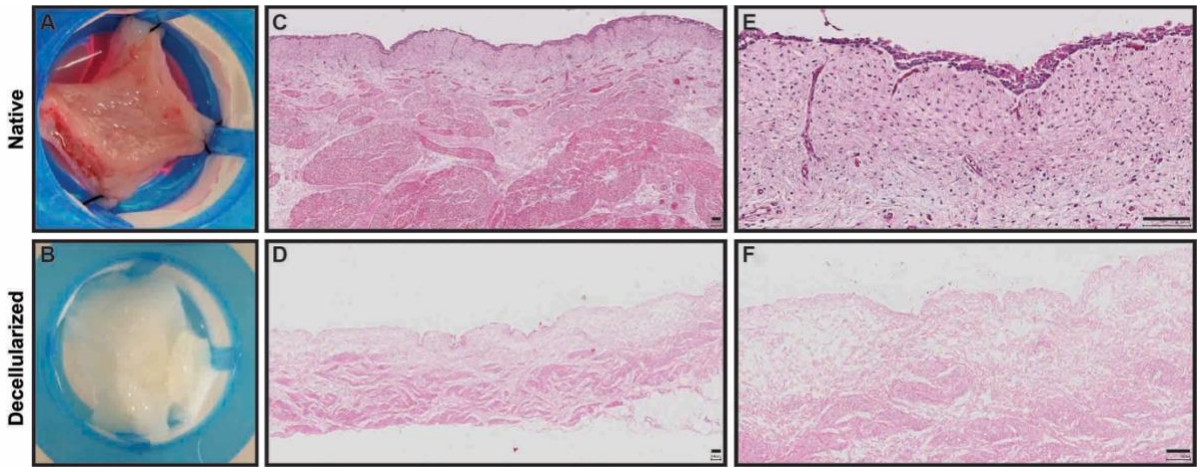

Figure 10. Macroscopic visualization and histological examination of native (A, C, E,) and decellularized (B, D, F) bladders. (A) Native bladder in a 1 cm × 1 cm × 0.5 cm square. **(B)** Decellularized pig bladder in a 1 cm × 1 cm × 0.5 cm square. **(C, D, E, F)** H&E stains: native **(C)** and decellularized **(D)** bladder with 4X magnification. **(E)** Urothelium, lamina propria and submucosa of native bladder square with 20X magnification. **(F)** Lamina propria and submucosa of decellularized bladder square with 20X magnification.
Scale bars in panel C, D, E and F represent 100 μm.

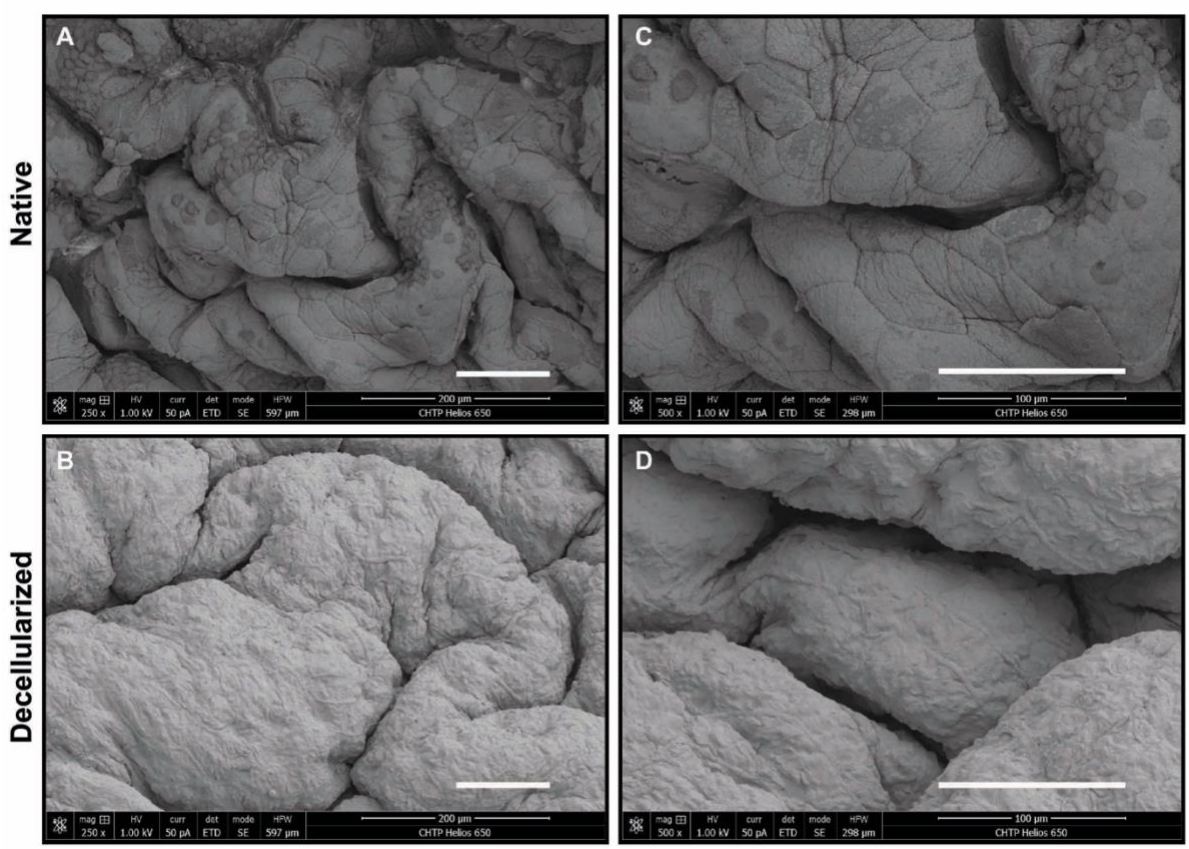

Figure 11. Structural analysis of native (A, C) and decellularized (B, D) bladders. SEM images: urothelium of native bladder **(A)** (250X) and **(C)** (500X). Hexagonal cell characteristic of the umbrella cells from the urothelium was clearly showed. Basement membrane (lamina propria) of decellularized bladder **(B)** (250X) and **(D)** (500X). No hexagonal cell characteristic was seen indicates the complete removal of umbrella cells. Microarchitecture of the bladder ECM was preserved (no significant structural changes were observed on the basement membrane) comparing between native **(A) (C)** and decellularized bladder **(B) (D)**.
All scale bars represent 100 μm.

3.2.3 Structural protein and ECM-bound growth factors are preserved after decellularization of bladder

Once bladders were decellularized and remaining DNA was within accepted ranges, I wanted to evaluate the remaining full-protein profile of the decellularization bladder ECM. Bother native and decellularized bladders were evaluated using LC-MS/MS (Table 3 and 4).

Specific structural proteins that maintain the integrity of the impermeable bladder surface (formation of basal membrane and lamina propria) such as elastin, collagen, laminin and fibronectin (52) (53) (54) were preserved in decellularizated bladders compare to native bladders. Biglycan and agrin, proteins that are responsible for cell-matrix interactions (55) (56) were consistently found in both native and decellularized bladders. Cohesive proteins that link actin filaments and other support proteins: destrin and dystrophin (57) (58) were preserved during decellularization. Lumican, the protein that is responsible of epithelial cell migration and potential tissue repair was seen in both native and decellularized bladder matrix (59). Similar to previous proteomic evaluation of kidneys, ECM structural proteins – fubulins associate with basement membrane and elastic fibers and interact with many extracellular matrix constituents including fibronectin and laminins (49). Functional proteins - galectins, which has broad functions including mediation of cell-cell interaction, cell-matrix adhesion and transmembrane signaling in the ECM (50) were seen in both native and

decellularized bladders. Again, the existence of galectin may ensure the recellularization potency in future experiments.

Various growth factors such as latent-transforming growth factors, which are critical to tissue repairs (60) (61) and transforming growth factors that are responsible for epithelial cell differentiation (51) were well preserved using the optimized decellularization protocol developed in this study.

Table 3. Proteomic analysis of decellularized (Rattus norvegicus) bladder

Accession	Decellularized Bladder Protein	Coverage	Number of Peptides	Number of Unique peptides	MW [kDa]
Q99PD6	Agrin	1.020929045	3	3	208.5
O35568	alpha-internexin	3.366336634	2	0	56.1
Q6P686	Basal cell adhesion molecule	7.852564103	2	2	67.5
Q00918	biglycan	24.11924119	7	6	41.7
P31232	Calponin-1	46.12794613	15	13	33.3
P02454	Clusterin	30.20134228	15	15	51.3
Q9WUH4	Collagen alpha-1(I) chain	70.88781831	130	124	137.9
P02466	Collagen alpha-1(II) chain	11.69837914	12	6	134.5
P85972	Collagen alpha-1(III) chain	56.32262474	106	104	138.9
Q63532	Collagen alpha-1(V) chain	19.07608696	26	21	183.9
P13941	Collagen alpha-1(XI) chain	16.40798226	14	9	180.9
Q08290	Collagen alpha-2(I) chain	66.6909621	111	110	129.5
Q7M0E3	Cornifin-A	58.55263158	3	3	16.7
P09656	decorin	33.05084746	12	11	39.8
Q01129	Destrin	41.81818182	11	10	18.5
Q99J82	Dystrophin	11.36796301	29	29	425.6
P05371	EGF-containing fibulin-like extracellular matrix protein 1	22.10953347	6	6	54.6
P15800	Elastin	21.14942529	5	5	73.3
Q68FP1-2	Extracellular matrix protein 1	2.846975089	2	2	63.2
Q68FP1	Fibrinogen alpha chain	8.823529412	8	8	86.6
P47853	Fibrinogen beta chain	14.61377871	5	5	54.2
Q99372-8	Fibrinogen gamma chain	11.23595506	5	5	50.6
Q99372-7	fibronectin	14.4529673	25	25	272.3
Q99372-5	Fibulin-5	15.17857143	6	6	50.1
Q99372-2	Four and a half LIM domains protein 1	68.21428571	22	22	31.9
Q01177	Galectin-1	13.33333333	2	2	14.8
Q99372-6	Galectin-3	3.053435115	2	2	27.2
Q99372-4	Gelsolin	24.35897436	15	15	86
Q99372-3	Glycogen phosphorylase, brain form	13.96181384	13	11	96.1
Q99372	Glycogen phosphorylase, muscle form	11.28266033	9	7	97.2
P51886	Hemopexin	9.130434783	3	3	51.3
Q9JI03	Integrin alpha-1	5.338983051	7	7	130.7

Accession	Decellularized Bladder Protein	Coverage	Number of Peptides	Number of Unique peptides	MW [kDa]
B5DFC9	integrin alpha-7	4.933920705	5	5	124.1
P20909-6	Integrin beta-1	15.01877347	12	12	88.4
B5DFC9-2	Integrin beta-4	1.881571666	2	2	200.5
P20909-4	Integrin-linked protein kinase	31.4159292	15	15	51.3
P20909-5	Isoform 1 of Neuroplastin	16.72597865	5	5	31.3
P97546-3	Isoform 2 of Agrin	1.025641026	3	3	207.4
P20909-3	Isoform 2 of Collagen alpha-1(XI) chain	16.29955947	14	9	182.1
P97546-1	Isoform 2 of Elastin	22.3030303	5	5	69.1
P20909-1	Isoform 2 of Fibrinogen alpha chain	12.54545455	8	8	60.5
P20909-2	Isoform 2 of Fibrinogen beta chain	12.32604374	4	4	56.6
P21807	Isoform 2 of Fibronectin	14.45328865	24	24	262.6
Q9JI92	Isoform 2 of Gelsolin	25.99179207	15	15	80.9
P04937-4	Isoform 2 of Nidogen-2	17.61363636	4	4	20.1
Q9WVH8	Isoform 3 of Agrin	1.030927835	3	3	206.4
P49134	Isoform 3 of Collagen alpha-1(XI) chain	16.77053824	14	9	176.4
P14480	Isoform 3 of Elastin	21.17376295	5	5	73.2
P04937-3	Isoform 3 of Fibronectin	14.60032626	25	25	269.6
P04937-2	Isoform 3 of Neuroplastin	16.96750903	5	5	30.8
P04937-1	Isoform 4 of Agrin	1.026694045	3	3	207.3
Q642A6	Isoform 4 of Collagen alpha-1(XI) chain	17.21931355	14	9	171.3
P53534	Isoform 4 of Elastin	21.52046784	5	5	71.8
P11762	Isoform 4 of Fibronectin	15.18235793	25	25	259.2
P06399-2	Isoform 5 of Agrin	1.025115325	3	3	207.6
P14480-2	Isoform 5 of Collagen alpha-1(XI) chain	17.09994223	14	9	172.5
P97546-2	Isoform 5 of Elastin	22.33009709	5	5	69
P05539	Isoform 6 of Agrin	1.023017903	3	3	208
P02680-2	Isoform 6 of Collagen alpha-1(XI) chain	17.61904762	14	9	166.7
P11530	Isoform 6 of Elastin	21.54566745	5	5	71.7
P09812	Isoform 7 of Elastin	22.71604938	5	5	67.6
P02680-1	Isoform 8 of Elastin	22.74412855	5	5	67.6
P20059	Isoform Alpha-7X1A of Integrin alpha-7	5.017921147	5	5	121.6

Accession	Decellularized Bladder Protein	Coverage	Number of Peptides	Number of Unique peptides	MW [kDa]
P06399	Isoform Alpha-7X1C of Integrin alpha-7	5.204460967	5	5	117.4
Q9ESS6	Isoform Gamma-A of Fibrinogen gamma chain	11.4416476	5	5	49.6
Q9EQP5	Lamin-B1	6.473594549	4	3	66.6
P70615	laminin subunit beta-2	29.65019434	39	39	196.3
P08460	Latent-transforming growth factor beta-binding protein 1	4.497663551	6	6	186.5
P35446	Lumican	20.71005917	5	5	38.3
P18614	Neuroplastin	11.95928753	5	5	43.9
Q63258-3	Nidogen-1	5.864197531	2	2	35.6
Q63258-2	Nidogen-2	18.26647564	15	15	152.9
Q63258	osteoclast-stimulating factor 1	11.68224299	2	2	23.7
Q63321	Peripherin	15.38461538	9	5	53.5
P23565	Plasminogen	21.79802956	13	13	90.5
P08699	Procollagen-lysine,2-oxoglutarate 5-dioxygenase 1	3.983516484	2	2	83.6
Q62894	prolargin	7.692307692	2	2	43.2
Q64632	Serine protease inhibitor Kazal-type 1-like	34.17721519	4	4	8.6
P25304-3	Spondin-1	5.576208178	2	2	90.7
P25304-4	Syntenin-1	15.33333333	2	2	32.4
P25304-2	Transforming growth factor beta-1-induced transcript 1 protein	24.94577007	8	8	50.1
P25304-5	transgelin	73.6318408	19	19	22.6
P25304-6	Vinculin	61.35084428	65	65	116.5
P25304-1	von Willebrand factor A domain-containing protein 1	13.97590361	3	3	44.8

Table 4. Proteomic analysis of native (Rattus norvegicus) bladder

Accession	Decellularized native Protein	Coverage	Number of Peptides	Number of Unique peptides	MW [kDa]
O35568	Agrin	2.603369066	4	4	208.5
Q99PD6	Angiotensinogen	9.853249476	4	4	51.9
Q00918	Basal cell adhesion molecule	7.051282051	4	4	67.5
P02454	biglycan	26.82926829	7	6	41.7
P02466	Bone marrow proteoglycan	8.370044053	2	2	25.1
P31232	Calponin-1	42.08754209	12	10	33.3
P13941	Cathepsin D	16.70761671	5	5	44.7
Q7M0E3	Chondroitin sulfate proteoglycan 4	1.418744626	2	2	251.8
P85972	Collagen alpha-1(I) chain	73.98485891	115	112	137.9
P11762	Collagen alpha-1(II) chain	15.08104299	16	11	134.5
Q01129	Collagen alpha-1(III) chain	64.38824334	107	105	138.9
Q08290	Collagen alpha-1(V) chain	25.43478261	35	29	183.9
Q9WUH4	Collagen alpha-1(XI) chain	9.201773836	10	5	180.9
P15800	Collagen alpha-1(XII) chain	6.624605678	2	2	32
B5DFC9-2	Collagen alpha-2(I) chain	70.91836735	90	88	129.5
P14480	decorin	43.22033898	16	15	39.8
Q68FP1-2	Destrin	63.03030303	11	10	18.5
P51886	Dystrophin	11.09600218	34	34	425.6
Q68FP1	EGF-containing fibulin-like extracellular matrix protein 1	29.00608519	8	8	54.6
P14480-2	Elastin	20.8045977	5	5	73.3
Q9QX79	Extracellular matrix protein 1	10.3202847	5	5	63.2
P06399	Fetuin-B	32.01058201	6	6	41.5
P02680-2	Fibrinogen alpha chain	27.87723785	20	20	86.6
P02680-1	Fibrinogen beta chain	35.6993737	14	14	54.2
P47853		27.19101124	11	11	50.6
P04937-4	fibronectin	25.3532499	49	49	272.3
P04937-2	Fibulin-5	20.3125	9	9	50.1
P04937-3	Four and a half LIM domains protein 1	38.57142857	11	11	31.9
Q9JI03	Galectin-1	51.11111111	6	6	14.8
P04937-1	Galectin-3	7.633587786	2	2	27.2
Q99J82	Gelsolin	33.33333333	21	21	86
Q9EQP5	Hemopexin	15	6	6	51.3
Q5XFX0	Integrin alpha-1	9.830508475	11	11	130.7
P08932	integrin alpha-7	2.907488987	3	3	124.1
Q99372-5	Integrin beta-1	13.89236546	11	11	88.4
Q99372-2	Integrin-linked protein kinase	25	12	12	51.3

Accession	Decellularized native Protein	Coverage	Number of Peptides	Number of Unique peptides	MW [kDa]
Q99372-6	Isoform 2 of Agrin	2.615384615	4	4	207.4
Q99372-4	Isoform 2 of Collagen alpha-1(XI) chain	9.140969163	10	5	182.1
Q99372-3	Isoform 2 of Elastin	21.93939394	5	5	69.1
Q99372	Isoform 2 of Fibrinogen beta chain	32.60437376	13	13	56.6
Q9WVH8	Isoform 2 of Fibronectin	25.76455802	48	48	262.6
Q2LAP6	Isoform 2 of Gelsolin	35.56771546	21	21	80.9
P01048	Isoform 2 of Nidogen-2	38.06818182	6	6	20.1
P24268	Isoform 3 of Agrin	2.628865979	4	4	206.4
B5DFC9	Isoform 3 of Collagen alpha-1(XI) chain	9.40509915	10	5	176.4
P05539	Isoform 3 of Elastin	20.82853855	5	5	73.2
P20059	Isoform 3 of Fibronectin	25.61174551	49	49	269.6
P49134	Isoform 4 of Agrin	2.618069815	4	4	207.3
Q01177	Isoform 4 of Collagen alpha-1(XI) chain	9.656777196	10	5	171.3
P18292	Isoform 4 of Elastin	21.16959064	5	5	71.8
P11530	Isoform 4 of Fibronectin	26.63273961	49	49	259.2
Q62894	Isoform 5 of Agrin	2.61404408	4	4	207.6
P20909-6	Isoform 5 of Collagen alpha-1(XI) chain	9.589832467	10	5	172.5
P01015	Isoform 5 of Elastin	21.96601942	5	5	69
P18614	Isoform 6 of Agrin	2.608695652	4	4	208
P20909-4	Isoform 6 of Collagen alpha-1(XI) chain	9.880952381	10	5	166.7
P20909-5	Isoform 6 of Elastin	21.19437939	5	5	71.7
P20909-3	Isoform Gamma-A of Fibrinogen gamma chain	27.68878719	11	11	49.6
P20909-1	Isoform Short of Collagen alpha-1(XII) chain	8.015267176	2	2	25.4
P20909-2	kininogen-1	5.320813772	3	1	70.9
Q63189	laminin subunit beta-2 [	38.14547474	55	55	196.3
P70560-2	Latent-transforming growth factor beta-binding protein 1	1.752336449	3	3	186.5
P08699	Lumican	33.72781065	10	10	38.3
P37805	Nidogen-1	5.864197531	2	2	35.6
Q9ESS6	Nidogen-2	16.26074499	17	17	152.9
Q566D0	Peripherin	6.623931624	4	1	53.5
P70560-1	Plasminogen	13.1773399	8	8	90.5
P21807	Procollagen C-endopeptidase enhancer 1	5.555555556	2	2	50.2
Q75WE7	prolargin	24.40318302	10	10	43.2
P08460	Prothrombin	12.96596434	7	7	70.4
O08628	Testin	20.0477327	9	9	47.6
P08934-1	T-kininogen 1	18.60465116	5	5	47.7

Accession	Decellularized native Protein	Coverage	Number of Peptides	Number of Unique peptides	MW [kDa]
Q63258	T-kininogen 2	23.25581395	7	5	47.7
P25304-3	Tenascin	27.76572668	10	10	50.1
P25304-4	transgelin	66.16915423	16	16	22.6
P25304-2	Transgelin-2	24.12060302	6	6	22.4
P25304-5	Transgelin-3	7.537688442	2	0	22.5
P25304-6	Uroplakin-1b	6.923076923	2	2	29.8
P25304-1	Vinculin	55.15947467	53	53	116.5
Q00657	von Willebrand factor A domain-containing protein 5A	5.96107056	4	4	91.4

3.3 Optimization of kidney ECM recellularization

In order to test viabilities of different cells within the decellularized kidney ECM and reduce experimental uncertainties, we decided to perform single cell-type recellularization to each decellularized kidney ECM sections. Human endothelial cells (HUVEC) were reseeded onto the sectioned decellularized rodent kidney ECM (Figure 12 - A) as described in section 2.5.2. As seen in Figure 12 - B, the H&E staining of a cross section of panel - A showed that endothelial cells were only positioned around a vascular structure and no cellular distributions were seen in other areas (20X magnification).To ensure these cells were human endothelial cells but not pre-existed animal cells, the section of the same area was stained with Anti-CD31 and the positive stains demonstrated successful recellularization of human endothelial cells around the tubule-like structure (Figure 12 – C, 10X magnification). I considered the key point of success owes to the viability of the cells; the cells being reseeded were of early passage (P3). It is recorded that previous late passage (P12 and P15) HUVEC-reseedings were performed under the same conditions (total cell number, incubation time and cell culture condition) but they were not successful. Therefore, I assume that the success of HUVEC-reseeding to kidney ECMs is highly associated with cell passage, the earlier the passage, the more likely a successfully reseeding can be performed. Researchers should always make account of cell viability for future recellularization. It is also noteworthy that more areas were stained in panel C than in panel B, possible reason of this observation could be the slide obtained in panel C was sectioned deeper than in that of panel B. Different sections of the tissue could

show different cellular distribution since cell penetration after reseeding may not occur at the same time or with the same rate.

Human clear cell carcinoma cells (Caki-1) were reseeded onto the sectioned decellularized rodent kidney ECM (Figure 13 - A) as described in section 2.5.2. As seen in Figure 13 - B, the H&E staining of a cross section of panel - A showed cancer cells were penetrating and forming aggregates in the decellularized ECM (Figure 13 – B, 10X magnification). In panel – B and C (30X magnification), there are more gaps between cancer cells and the adjacent decellularized ECM compared to areas with less cancer cells being reseeded. Also, the cancer cells were randomly aggregating into clumps at different areas of the tissue, which mirrored the characteristic of cancers. Comparing between Figure 12 – B and Figure 13 – B, the appearances of ECM were different when reseeded with different cells. More organized structures were seen in the ECM recellularized with normal human cells (Figure 12 – B) and more irregular structures were seen in the ECM reseeded with cancer cell. This phenomenon was observed in concurrent experimental duplicates (not shown) and indicated that different cells affect the decellularized ECM differently. Human embryonic cells (HEK293) were also reseeded onto the decellularized kidney ECM as described in section 2.5.2 but unfortunately after trying twelve times, no viable cells were observed on the decellularized tissues (evaluation using H&E) (result not shown).

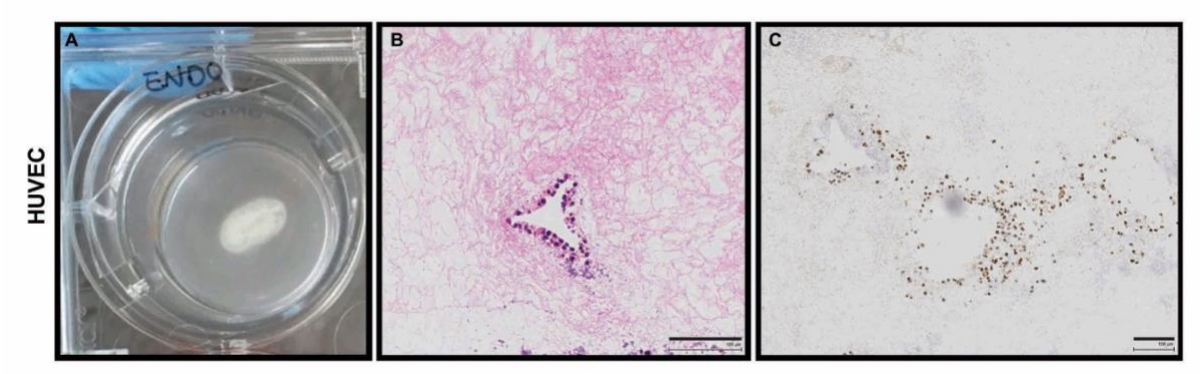

Figure 12. Macroscopic visualization and histological examination of recellularized kidney. (A) Longitudinal section of a recellularized rodent kidney (recellularized with HUVEC). **(B)** Haematoxylin & Eosin stains of the recellularized rodent kidney (20X). **(C)** Immunohistochemistry: Anti-CD31 staining of the same area as in **(B)** with a 10X magnification
Scale bars in panel B and C represent 100 μm.

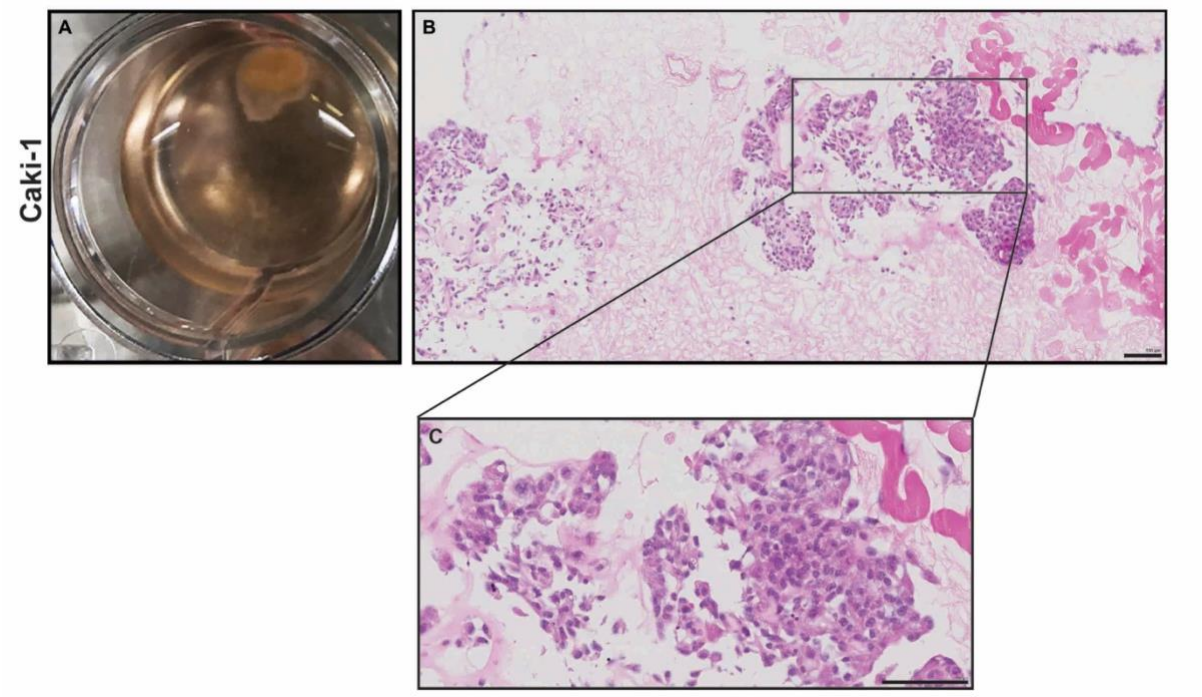

Figure 13. Macroscopic visualization and histological examination of recellularized kidney. (A) Cross section of a recellularized rodent kidney (recellularized with Caki-1 cell lines). **(B)** Hematoxylin & Eosin stains of the recellularized rodent kidney (10X magnification). **(C)** magnified area of **(B)** (30X magnification).
Scale bars in Panel B and C represent 100 μm.

3.4 Optimization of bladder ECM recellularization

a) Single cell-type recellularization

In order to test viabilities of different cells within the decellularized bladder ECM and reduce experimental uncertainties, we decided to perform single cell-type recellularization to each decellularized bladder ECM squares. Human urothelial cells (SV-HUC) were reseeded onto the urothelium of the sectioned decellularized pig bladder ECM (Figure 14 – A) as described in section 2.5.3. The H&E staining showed cells were uniformly positioned on the surface of the urothelium showing few layers (Figure 14 – D, 10X magnification). It was observed that the reseeded urothelial cells were aligning at the urothelium in an organized manner and were not penetrating the basement membrane. It showed in both panel D and G (20X magnification) that the recellularization of human urothelial cells did not jeopardize the integrity of the basement membrane. Human UM-UC-3 cancer cells were reseeded onto the urothelium of the sectioned decellularized pig bladder ECM (Figure 14 – B) as described in section 2.5.3. The H&E staining showed cells were aligning at the urothelium and some were penetrating into the ECM (Figure 14 – E, 10X magnification). Also, the cancer cells were changing the decellularized ECM while entering the stroma (Figure 14 – H, 20X magnification). Different from the organized positioning pattern of human urothelial cells, bladder cancer cells were randomly aligning (cells are layering up) at the urothelium, which mirrors the characteristics of invasive bladder cancer. Human fibroblasts were reseeded onto the decellularized pig bladder ECM squares (Figure 14 – C) as described in section 2.5.3. The H&E staining

showed cells were scattered throughout almost all the stromal layer (Figure 14 – F, 10X magnification).

Overall, single cell-type recellularization of bladder ECM was successfully generated with human urothelial cells (SV-HUC), fibroblasts and bladder cancer cells (UM-UC-3), respectively. According to several tested protocols described in Appendix E, cell number, media used when reseeding and time of incubation (days) all matter to the outcomes of the recellularization. It clearly shows in Figure 13 that comparing between reseeding SV-HUC and UM-UC-3, human urothelial cells were uniformly aligning on the urothelium without penetrating the basement membrane while bladder cancer cells were unevenly aggregating on the urothelium with formation of thick layers and trying to penetrate more into the basement membrane. As for fibroblasts recellularization, it was observed that cells were randomly penetrating the stroma and it demonstrated the low density of the bladder ECM. It was speculated that fibroblasts were consuming the decellularized bladder ECM to make rooms for their own penetration. These phenomena explain the nature/property of different cells and more importantly, illustrated the possible cell-guiding feature of the decellularized bladder ECM. Interestingly, morphological changes were observed only on the bladder ECM that was reseeded with fibroblasts. The edges of the ECM curled up (Figure 14 - C) thus created a small cave in the center, which mirrors the fact that fibroblasts tend to have cell traction during proliferation (62). Human endothelial cells (HUVEC) were also reseeded on the stroma of the decellularized bladder ECM as described in

section 2.5.3 but unfortunately after trying eight times, no viable cells were observed on the tissue when reseeded alone (evaluation using H&E) (result not shown).

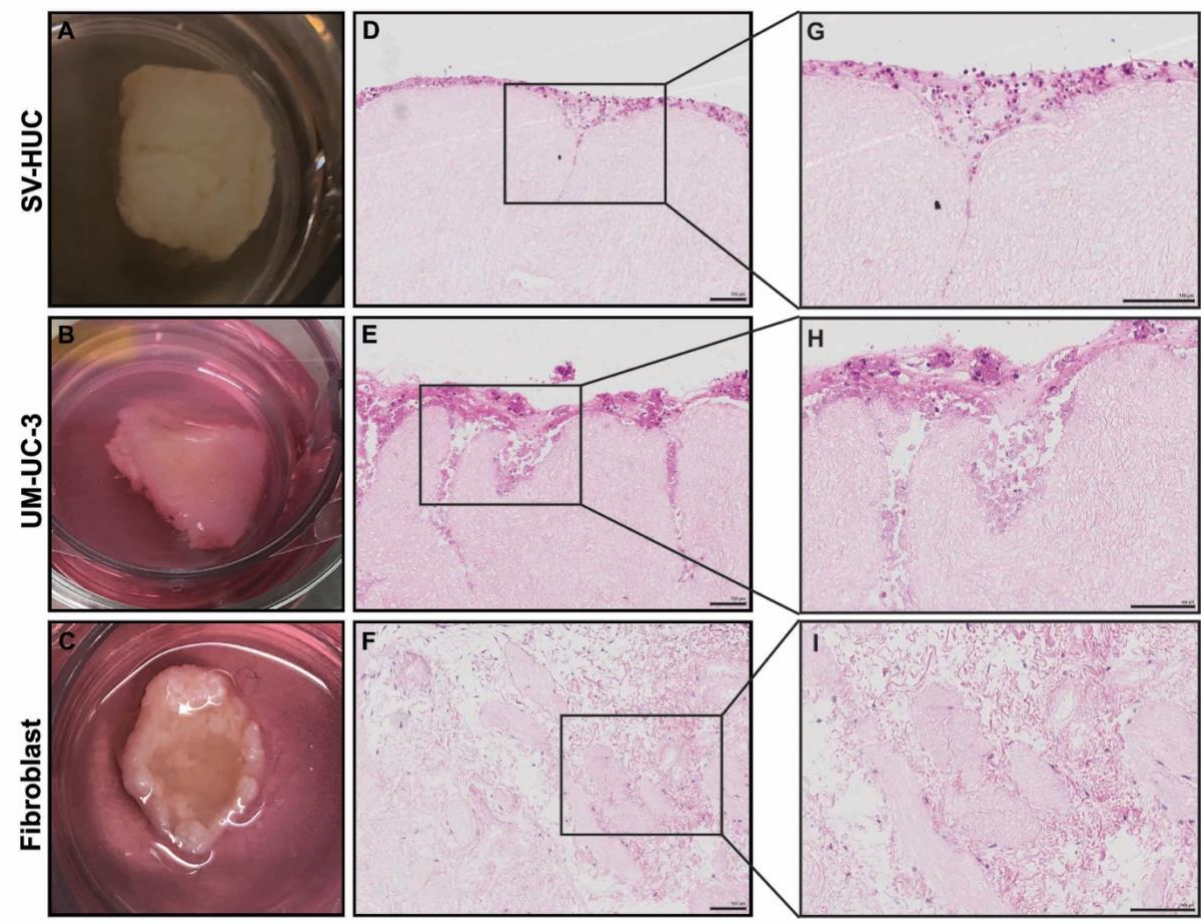

Figure 14. Macroscopic visualization (A, B, C) and histological examination (D, E, F) of recellularized bladder. Recellularized pig bladder with surface area of 1cm^2. **(A)** Recellularized with SV-HUC. **(B)** Recellularized with UM-UC3. **(C)** Recellularized with primary fibroblast. Hematoxylin & Eosin stains of the recellularized pig bladder (10X): **(D)** Cross section of **(A)**, **(E)** Cross section of **(B)**, and **(F)** Cross section of **(C).** Hematoxylin & Eosin stains of the recellularized pig bladder (30X): **(G)** magnified image of **(D)**, **(H)** magnified image of **(E)**, and **(I)** magnified image of **(F).**
Scale bars in panel D, E, F, G, H and I represent 100 μm.

b) Multi cell-type recellularization

Human endothelial, fibroblasts, and urothelial cells were reseeded together onto a decellularized pig bladder ECM square (Figure 15 – B) (endothelial and fibroblast cells onto the stroma while urothelial cells onto the urothelium, as described in section 2.5.3. As seen in Figure 15 – D, multi cell-type recellularization of bladder ECM was successfully generated with human endothelial cells (HUVEC), human urothelial cells (SV-HUC) and primary fibroblasts. According to several tested protocols described in Appendix F, cell ratio (HUVEC: Fibroblast: SV-HUC), media used when reseeding and time of incubation (days) all matter to the outcomes of the recellularization. Similar to single cell-type recellularization, the edges of the bladder ECM also curled up (Figure 15 – B) due to existence of fibroblasts. It clearly shows in Figure 15 - D that cells are reseeded/distributed on both sides of the basement membrane and showed different patterns. This observation illustrated that the previous decellularization protocol did not compromise the integrity of the basement membrane and proved its effectiveness. In order to identify cell type and ensure whether or not cellular distributions were related to cell types. Positive IHC staining of Anti-CD31 antibody (specifically react with human CD31) confirmed that HUVECs but not porcine cells were distributed around multiple vessel-like structures (Figure 15 – E, 20X magnification). Similarly, positive IHC staining of Anti-Vimentin antibody (specifically react with human vimentin) confirmed that human fibroblasts but not porcine cells were uniformly distributed in the stromal layer (Figure 15 – F, 20X magnification). Although SV-HUC was not stained with its corresponding antibody, they were the only reseeded cells on the urothelium side (HUVEC and fibroblast were reseeded on the stromal side). In this

case, the unstained cells could only be SV-HUC (Figure 15 – D & F, 20X magnification). Overall, it was clear that HUVECs, fibroblasts and SV-HUCs were growing independently without interfering with each other. This finding indirectly proved the bladder immersion protocol is valid.

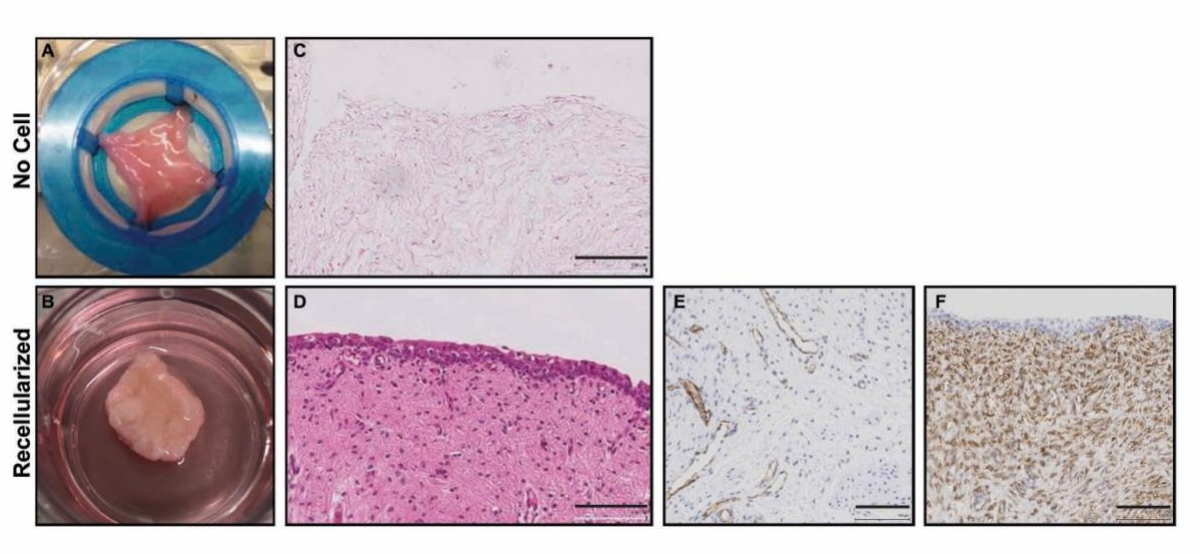

Figure 15. Macroscopic visualization and histological examination of decellularized (A, C) and recellularized (B, D, E, F) bladders. (A) Decellularized pig bladder with surface area of 1cm^2. **(B)** Recellularized pig bladder with surface area of 1cm^2. **(C)** Hematoxylin & Eosin stains of the decellularized pig bladder (20X). **(D)** Hematoxylin & Eosin stains of the recellularized pig bladder (20X, recellularized with HUVECs, primary fibroblasts and SV-HUCs). **(E, F)** Immunohistochemistry: **(E)** Anti-CD31 staining of recellularized pig bladder with a 20X magnification and **(F)** Anti-Vimentin staining of recellularized pig bladder with a 20X magnification.
Scale bars in panel C, D, E and F represent 100 μm.

3.5 Human fibroblast demonstrated ECM penetrating capacity

As described in section 2.6 (b) and 3.4 (a), cell penetration of fibroblast cells was measured using digital ruler from the H&E slides (cross section of the tissue) and the penetration rate was calculated according to each tissue's thickness. With measurement of four duplicate recellularizations, human fibroblast cells had **1)** penetrated 332.7 µm in a tissue of 3500 µm thickness (mean penetration rate is 0.011 µm/min); **2)** penetrated 453.6 µm in a tissue of 2400 µm thickness (mean penetration rate is 0.015 µm/min); **3)** penetrated 423.4 µm in a tissue of 4600 µm thickness (mean penetration rate is 0.014 µm/min) and **4)** penetrated 302.4 µm in a tissue of 3800 µm thickness (mean penetration rate is 0.010 µm/min). Therefore, fibroblasts had a mean penetration rate in decellularized bladder ECM of 0.013 µm/min with a standard deviation of 0.0064 µm/min, n=4.

Since the mean penetration rate of fibroblast in decellularized bladder ECM is 0.013 µm/min $\pm$ 0.0064 µm/min, statistical analysis was performed using the Student's t-test. H_0: the fibroblasts' penetration rate in decellularized bladder ECM is zero. H_α: the fibroblasts' penetration rate in decellularized bladder ECM is bigger than zero. Under null hypothesis, T=4.063 and p=0.013<0.05. Therefore, p<0.05 rejects H_0. It approved the alternative hypothesis that the calculated fibroblasts' penetration rate in decellularized bladder ECM was statistically significant.

However, the fibroblasts' mean penetration rate was calculated (μm/min) based on current recellularization duplicates. With this information, researchers would have an estimation for future fibroblasts' reseedings under the same conditions. Since corresponding media was replaced on a daily basis and frequent movements could possibly have some interference to cell growth in the ECMs, therefore, extra cautious was required when handling and disturbing during incubation should be minimized.

Chapter 4: Discussion

Currently, little information is available regarding organ/tissue derived ECM in the application of 3D *in vitro* urogenital tumor models. However, other 3D tumor models were recently described and could potentially share similar principles. Previous studies showed that decellularized ECM produced from decellularized rodent lungs appeared to be a promising 3D metastatic breast tumor model with correct spatial arrangement, biomechanical properties and biocompatibilities (63). Altered expression of biomarkers was observed in this model compared to in a 2D system. Another study showed that a decellularized patient tissue-derived (brain) ECM were used to generate research upon invasion route of glioblastoma (64). Glioblastoma cells exhibited different cell behaviors in the 3D environment compare to that of in 2D condition. These studies illustrated that 3D tumor models are essential since they bridge the gap between 2D models and corresponding “real-life” *in vivo* scenarios. Therefore, superior physiologic/biologic and clinical relevance can be achieved with the development of 3D tumor models for urogenital cancers. Rodent kidneys and porcine bladder squares were chosen as starting materials of the 3D scaffolds, as they share many anatomical, histological and physiological similarities with human beings (65) (66).

In this study, a protocol with combined physical and chemical approaches for the perfusion decellularization of whole rat kidney was established, representing a preliminary step toward the building of a bioengineered scaffold for kidney tumor

models. The kidney was secured in an in-house developed bioreactor as described in section 2.2.1 during decellularization. After testing, the actual time used per decellularization cycle is 20% longer than that described in a similar study (38), which has longer exposure of Triton X-100 than ours, and with no disclosure of the cycle numbers needed. However, although complete cell removal was revealed, our study demonstrated more orderly distributed renal microarchitecture with intact tubules and uniform ECM density in the H&E evaluations. Our study suggests that slower decellularization process (less peristaltic force introduced) may apply less disruption to the fine ECM microstructures. On the other hand, slower peristalsis results in longer exposure of renal ECM to detergents. It has been reported that prolonged exposure of ionic detergents may denaturize structural and functional ECM proteins as well as alter certain biomechanical properties, hence, this prolonged exposure may potentially decrease/inhibit cell-ECM interactions and jeopardize ECM integrity (33) (67). It is key to apply proper detergent exposure and peristaltic force to ensure the future applicability of the decellularized ECM (i.e. recellularization, characterization).

The bioreactor in our study was used for decellularization and we performed recellularization by hand. Previous studies utilize bioreactors for reseeding as well (68). For example, HUVECs can be reseeded through renal arteries of decellularized kidneys resulting in re-endothelialized kidney constructs across the entire kidney section including interlobar, arcuate arteries, glomeruli and peritubular capilaries (68). In our study, reseeded HUVECs were only found lining around a few circular structures without any involvement of renal glomeruli as described in section 3.3. The

differences in results may be due to different recellularization protocols. The perfusion approach provided long-lasted reseeding into the renal vasculature and the manual approach could only position cells on the surface of the renal vasculature. In this case, it is suggestive that cells reseeded by perfusion are more likely to reside in the kidney than that performed by hand. On the other hand, cell numbers being reseeded using bioreactors require very high concentration of cells that is much more than in our study (68). Therefore, we speculate that sufficient cell-number may be crucial for successful kidney ECM recellularization.

One of the novelties in this study is that to our knowledge, we are the first to successfully reseed renal cancer cells onto the decellularized kidney ECM. As described in section 3.3, ccRCC cell line was successfully reseeded under various conditions and formed aggregates in different locations of the decellularized ECM. It demonstrated that metastatic kidney cancer cells can be grown and proliferated on a 3D platform without strict conditions. It is speculated that these cancer cells may grow in an integrative and interactive manner with other cells in 3D conditions as well. Previous studies described the reseeding of colon (69) and breast cancer cells (70) to their corresponding organ specific decellularized ECMs. Although the reseeding principles are similar to that of our study, the integration of cancer cells to a matrix was not observed within the colon cancer cells reseeding model (69) which was distinct from the *in vivo* scenario. Meanwhile, integration of cells to the ECM was seen in a breast cancer model which demonstrated mimicry to the *in vivo* situation. Despite the methodology that injected cancer cells inside the ECM, which bypassed the

initiation of cell penetration, this study lacked evidence showing cell-ECM interactions (70). In our study, metastatic kidney cancer cells formed significantly larger interconnected multicellular aggregates (100 – 200 μm in size) inside the decellularized ECM with the methodology of loading cells onto the matrices. Obvious cell integration was observed. It is suggestive that our model achieved better mimicry of the *in vivo* condition with presentation of cell-ECM interactions during cell growth.

On the other hand, attempts to reseed the decellularized kidney ECM with HEK293 cells by hand was not successful. Currently, our bioreactor does not allow for infusion of cells. Modification of our bioreactor to allow for distribution of cells in addition to detergents may allow for integration of cells to the renal ECM. Therefore, future studies are planned to perform recellularization by perfusion after modification of our bioreactor. Also, a combination of cells (cancerous, endothelial and embryonic) can be reseeded together using perfusion approach to observe cellular distributions.

During the establishment of a bladder cancer model, a protocol with combined physical and chemical approaches for the immersion decellularization of porcine bladder squares was established, representing a preliminary step toward the building of a bioengineered scaffold for bladder tumor models. A recent study performed perfusion decellularization to rabbit bladders with non-ionic detergent passing through the urethra (71). Despite have different organ sources, we performed immersion decellularization with salt solutions and achieved satisfactory results with histological and SEM evaluations as described in section 3.2. Perfusion decellularization was not

performed on porcine bladder because it was not efficient to do so with such a sizable organ. Instead, we sectioned it into equal squares for easier manipulation. In addition, we tested non-ionic detergents as described in a related study (71) with immersion approach but did not achieve similar decellularization results. The main difference was organ thickness. Hence, these results suggest that non-ionic detergents may not pass through thicker tissues easily during immersion decellularization and alternative reagents may be required when using these tissues.

Previous studies demonstrated sophisticated procedures and set-ups to rebuild a functional bladder involving the use of stem cells and various scaffolds (72) (73). Since our focus is to create a tumor mimicry of *in vivo* conditions instead of reforming the organ functionality, both normal/mortal and cancerous cells were reseeded to the decellularized bladder ECM. One of the novelties of this study is that, to our knowledge, we are the first group successfully reseed urothelial cancer onto the decellularized bladder ECM. As described in section 3.4, UM-UC3 cell line was successfully reseeded on the urothelium of the bladder and showed obvious invasiveness compare to that reseeded with urothelial cells. Multi-cell layers formed on the urothelium as bladder cancer during cell reseeded. Also, the ECM underneath was partially degraded by cancer cell invasion. Thus, it demonstrated the aggressiveness of ccRCC, which cannot be observed in a 2D system. These results reveal that this model better translates the cancer biology and serves the purpose of bridging the gap between 2D models and “true” scenarios.

In this study, benign urothelial cells (SV-HUC) were also reseeded by hand and majority of cells were observed lining on the urothelium without penetrating the basement membrane. Similar study with by-hand recellularization approach showed almost identical results (74) show that the bladder decellularization protocol described in section2.2.3 preserves the integrity of the basement membrane.

Cell migration is a key process during the development of tissue (75). Most cell migration assays were performed in 2D models and very few studies of cell movements were generated in 3D scenarios. In our study, we observed fibroblasts' penetration during bladder recellularization and since fibroblast plays a vital role in cancer initiation, invasion and metastasis (76), I explored their penetration pattern quantitatively. A related study performed fibroblast recellularization by-hand onto a decellularized bladder ECM and showed little cell penetration to the stroma (77). In our study, we successfully reseeded fibroblasts onto stroma of the bladder and incubated two times longer than that of the related study. Significant cell penetration was observed as described in section 3.5, which suggests that our model maintained the appropriate environment for cell growth.

This study demonstrates the success of multi-type cell reseeding (HUVECs + Fibroblasts + SV-HUCs) as described in section 3.4. Different cells were proved to be positioned at the correct locations: HUVECs and fibroblasts are in stroma when SV-HUCs are in the urothelium. This has not been shown previously and it suggests the potential to optimize it into a bladder's replica to mimic clinical conditions.

Tumor progression is highly associated with biochemical and mechanical cues provided by the ECM (78) (79). To accurately produce a urogenital tumor model from decellularized ECMs, the ECMs' composition is pivotal since it provides those cues for cell growth. On the other hand, ECM integrity is also important since cell proliferation is higher on more rigid surface (80), which explained the fact that cells attach more easily in 2D petri-dish than in 3D model. It further illustrates the reason why 3D tumor models mimic the *in vivo* condition better than that of 2D system. In the present study, decellularized kidney and bladder ECM were characterized/profiled as described in sections 3.1.3 and 3.2.3. Notably, the comprehensive full-protein profile of decellularized ECMs (kidney and bladder) has not been documented before and it demonstrates high compositional similarities (structural, functional proteins and certain growth factors) compare to that of native organs based on the measured coverage. This finding validated the effectiveness of our established decellularization protocols and set the foundation of successful cell proliferation after recellularization.

Above all, our *in vitro* urogenital tumor models have several advantages. **1)** The scaffolds were derived from biological tissues that maintain native biocompatibility, biodegradability and certain mechanical properties for cell growth. **2)** The scaffolds were cost-effective since they were retrieved from animal organs supposed to be discarded. **3)** High-throughput production can be achieved. **4)** Our models are potentially suitable for multi-cell type reseeding that provide biomimetic environment for cell growth. **5)** The models have potential to be used to culture patient-derived cells *in vitro* to predict therapeutic outcomes in a personalized manner.

Chapter 5: Conclusions and Future Directions

5.1 Summary

In summary, this thesis is a description of preliminary model-making methodologies with its related precautions and possible experimental obstacles. Within this study, tissue dissociation protocols of each organ were established and decellularization protocols for both kidneys and bladders were successfully optimized and established. The evaluation and characterization of the decellularized ECMs were accomplished with evidence of the preservation of structural proteins and growth factors. Afterward, the bladder ECM recellularization protocol was successfully optimized and established while the kidney ECM recellularization protocol was considered partially established due to inconsistent experimental reproducibility. In conclusion, this work establishes the model as proof-of-principle and sets the foundation for future patients' studies.

5.2 Future Directions

Moving forward, testing the validity and reliability of our model and recellularization is essential. Confirmation of the recapitulation of various genitourinary organs, with or without malignant cells, will be important to further develop our model for clinical use. Eventually, I envision our model being developed into a personalized medicine

platform in which patients' tumors are seeded in our model and then tested with various agents to determine optimal treatments. Optimization of our model may involve incorporation of the patient's own "normal" cells including immune cells. Genetic validation of the model can be performed and comparison between that and patients; tumor specimen can be generated. Eventually, with patients' cells being reseeded, different drug-testing assays can be established to identify the optimal treatment.

Bibliography

1. Canadian Cancer Statistics. Canadian Cancer Society's Advisory Committee on Cancer Statistics Toronto, ON: Canadian Cancer Society; 2017 [Available from: http://www.cancer.ca/en/cancer-information/cancer-type/bladder/statistics/?region=on.
2. Kindey Cancer Canada. A guide to kidney cancer 2017, Feb 1 [Available from: https://www.kidneycancercanada.ca/for-patients-and-caregivers/a-guide-to-kidney-cancer/.
3. Society CC. Canadian Cancer Statistics 2010, special topic: end of life care 2010 [Available from: http://www.cancer.ca/~/media/cancer.ca/CW/cancer%20information/cancer%20101/Canadian%20cancer%20statistics/Canadian-Cancer-Statistics-2010-EN.pdf?la=en.
4. Bladder Cancer Canada. Facing bladder cancer Toronto, ON2018 [Available from: https://bladdercancercanada.org/en/bladder-cancer-facts/.
5. Vickers AJ. Prediction models in cancer care. CA Cancer J Clin. 2011;61(5):315-26.
6. Riedl A, Schlederer M, Pudelko K, Stadler M, Walter S, Unterleuthner D, et al. Comparison of cancer cells in 2D vs 3D culture reveals differences in AKT-mTOR-S6K signaling and drug responses. J Cell Sci. 2017;130(1):203-18.
7. Edmondson R, Broglie JJ, Adcock AF, Yang L. Three-dimensional cell culture systems and their applications in drug discovery and cell-based biosensors. Assay Drug Dev Technol. 2014;12(4):207-18.
8. Breslin S, O'Driscoll L. The relevance of using 3D cell cultures, in addition to 2D monolayer cultures, when evaluating breast cancer drug sensitivity and resistance. Oncotarget. 2016;7(29):45745-56.
9. Xu X, Farach-Carson MC, Jia X. Three-dimensional in vitro tumor models for cancer research and drug evaluation. Biotechnol Adv. 2014;32(7):1256-68.
10. Jeong SY, Lee JH, Shin Y, Chung S, Kuh HJ. Co-Culture of Tumor Spheroids and Fibroblasts in a Collagen Matrix-Incorporated Microfluidic Chip Mimics Reciprocal Activation in Solid Tumor Microenvironment. PLoS One. 2016;11(7):e0159013.
11. Bogdanowicz DR, Lu HH. Multifunction co-culture model for evaluating cell-cell interactions. Methods Mol Biol. 2014;1202:29-36.
12. Gkretsi V, Stylianopoulos T. Cell Adhesion and Matrix Stiffness: Coordinating Cancer Cell Invasion and Metastasis. Front Oncol. 2018;8:145.
13. Katt ME, Placone AL, Wong AD, Xu ZS, Searson PC. In Vitro Tumor Models: Advantages, Disadvantages, Variables, and Selecting the Right Platform. Front Bioeng Biotechnol. 2016;4:12.
14. Lv D, Hu Z, Lu L, Lu H, Xu X. Three-dimensional cell culture: A powerful tool in tumor research and drug discovery. Oncol Lett. 2017;14(6):6999-7010.
15. Antoni D, Burckel H, Josset E, Noel G. Three-dimensional cell culture: a breakthrough in vivo. Int J Mol Sci. 2015;16(3):5517-27.

16. Mehta G, Hsiao AY, Ingram M, Luker GD, Takayama S. Opportunities and challenges for use of tumor spheroids as models to test drug delivery and efficacy. J Control Release. 2012;164(2):192-204.
17. Friedrich J, Seidel C, Ebner R, Kunz-Schughart LA. Spheroid-based drug screen: considerations and practical approach. Nat Protoc. 2009;4(3):309-24.
18. Sigaux N, Pourchet L, Breton P, Brosset S, Louvrier A, Marquette CA. 3D Bioprinting:principles, fantasies and prospects. J Stomatol Oral Maxillofac Surg. 2019;120(2):128-32.
19. Falguni Pati JJ, Jin Woo Lee, Dong-Woo Cho. Essentials of 3D Biofabrication and Translation2015. 440 p.
20. Knight E, Przyborski S. Advances in 3D cell culture technologies enabling tissue-like structures to be created in vitro. J Anat. 2015;227(6):746-56.
21. Cui X, Hartanto Y, Zhang H. Advances in multicellular spheroids formation. J R Soc Interface. 2017;14(127).
22. Yada E, Wada S, Yoshida S, Sasada T. Use of patient-derived xenograft mouse models in cancer research and treatment. Future Sci OA. 2018;4(3):FSO271.
23. Lampreht Tratar U, Horvat S, Cemazar M. Transgenic Mouse Models in Cancer Research. Front Oncol. 2018;8:268.
24. Hidalgo M, Amant F, Biankin AV, Budinska E, Byrne AT, Caldas C, et al. Patient-derived xenograft models: an emerging platform for translational cancer research. Cancer Discov. 2014;4(9):998-1013.
25. Dobrolecki LE, Airhart SD, Alferez DG, Aparicio S, Behbod F, Bentires-Alj M, et al. Patient-derived xenograft (PDX) models in basic and translational breast cancer research. Cancer Metastasis Rev. 2016;35(4):547-73.
26. Lai Y, Wei X, Lin S, Qin L, Cheng L, Li P. Current status and perspectives of patient-derived xenograft models in cancer research. J Hematol Oncol. 2017;10(1):106.
27. Cekanova M, Rathore K. Animal models and therapeutic molecular targets of cancer: utility and limitations. Drug Des Devel Ther. 2014;8:1911-21.
28. Langer R, Vacanti JP. Tissue engineering. Science. 1993;260(5110):920-6.
29. Mason C, Dunnill P. A brief definition of regenerative medicine. Regen Med. 2008;3(1):1-5.
30. O'Brien FJ. Biomaterials and Scaffold for tissue engineering. Materialstoday. 2011;14(3):88-95.
31. Ngangan AV, Waring JC, Cooke MT, Mandrycky CJ, McDevitt TC. Soluble factors secreted by differentiating embryonic stem cells stimulate exogenous cell proliferation and migration. Stem Cell Res Ther. 2014;5(1):26.
32. Monteiro AI, Kollmetz T, Malmstrom J. Engineered systems to study the synergistic signaling between integrin-mediated mechanotransduction and growth factors (Review). Biointerphases. 2018;13(6):06D302.
33. Gilpin A, Yang Y. Decellularization Strategies for Regenerative Medicine: From Processing Techniques to Applications. Biomed Res Int. 2017;2017:9831534.
34. Hinderer S, Layland SL, Schenke-Layland K. ECM and ECM-like materials - Biomaterials for applications in regenerative medicine and cancer therapy. Adv Drug Deliv Rev. 2016;97:260-9.

35. Crapo PM, Gilbert TW, Badylak SF. An overview of tissue and whole organ decellularization processes. Biomaterials. 2011;32(12):3233-43.
36. Keane TJ, Swinehart IT, Badylak SF. Methods of tissue decellularization used for preparation of biologic scaffolds and in vivo relevance. Methods. 2015;84:25-34.
37. Geerts S, Ozer S, Jaramillo M, Yarmush ML, Uygun BE. Nondestructive Methods for Monitoring Cell Removal During Rat Liver Decellularization. Tissue Eng Part C Methods. 2016;22(7):671-8.
38. Caralt M, Uzarski JS, Iacob S, Obergfell KP, Berg N, Bijonowski BM, et al. Optimization and critical evaluation of decellularization strategies to develop renal extracellular matrix scaffolds as biological templates for organ engineering and transplantation. Am J Transplant. 2015;15(1):64-75.
39. Hoshiba T, Lu H, Kawazoe N, Chen G. Decellularized matrices for tissue engineering. Expert Opin Biol Ther. 2010;10(12):1717-28.
40. Bard JB, Higginson K. Fibroblast-collagen interactions in the formation of the secondary stroma of the chick cornea. J Cell Biol. 1977;74(3):816-27.
41. Mansour JM, Welter JF. Multimodal evaluation of tissue-engineered cartilage. J Med Biol Eng. 2013;33(1):1-16.
42. Abrahamson DR, St John PL, Stroganova L, Zelenchuk A, Steenhard BM. Laminin and type IV collagen isoform substitutions occur in temporally and spatially distinct patterns in developing kidney glomerular basement membranes. J Histochem Cytochem. 2013;61(10):706-18.
43. Abrahamson DR. Development of kidney glomerular endothelial cells and their role in basement membrane assembly. Organogenesis. 2009;5(1):275-87.
44. Sebinger DD, Ofenbauer A, Gruber P, Malik S, Werner C. ECM modulated early kidney development in embryonic organ culture. Biomaterials. 2013;34(28):6670-82.
45. Pankov R, Yamada KM. Fibronectin at a glance. J Cell Sci. 2002;115(Pt 20):3861-3.
46. Schaefer L, Hausser H, Altenburger M, Ugorcakova J, August C, Fisher LW, et al. Decorin, biglycan and their endocytosis receptor in rat renal cortex. Kidney Int. 1998;54(5):1529-41.
47. Stokes MB, Holler S, Cui Y, Hudkins KL, Eitner F, Fogo A, et al. Expression of decorin, biglycan, and collagen type I in human renal fibrosing disease. Kidney Int. 2000;57(2):487-98.
48. Kim HY, Nelson CM. Extracellular matrix and cytoskeletal dynamics during branching morphogenesis. Organogenesis. 2012;8(2):56-64.
49. Timpl R, Sasaki T, Kostka G, Chu ML. Fibulins: a versatile family of extracellular matrix proteins. Nat Rev Mol Cell Biol. 2003;4(6):479-89.
50. Patnaik SK, Potvin B, Carlsson S, Sturm D, Leffler H, Stanley P. Complex N-glycans are the major ligands for galectin-1, -3, and -8 on Chinese hamster ovary cells. Glycobiology. 2006;16(4):305-17.
51. UniProt C. The universal protein resource (UniProt). Nucleic Acids Res. 2008;36(Database issue):D190-5.
52. Bosman FT, Stamenkovic I. Functional structure and composition of the extracellular matrix. J Pathol. 2003;200(4):423-8.

53. Wilson CB, Leopard J, Cheresh DA, Nakamura RM. Extracellular matrix and integrin composition of the normal bladder wall. World J Urol. 1996;14 Suppl 1:S30-7.
54. Brunner A, Tzankov A. The role of structural extracellular matrix proteins in urothelial bladder cancer (review). Biomark Insights. 2007;2:418-27.
55. Schonherr E, Witsch-Prehm P, Harrach B, Robenek H, Rauterberg J, Kresse H. Interaction of biglycan with type I collagen. J Biol Chem. 1995;270(6):2776-83.
56. Iozzo RV, Schaefer L. Proteoglycan form and function: A comprehensive nomenclature of proteoglycans. Matrix Biol. 2015;42:11-55.
57. Hatanaka H, Ogura K, Moriyama K, Ichikawa S, Yahara I, Inagaki F. Tertiary structure of destrin and structural similarity between two actin-regulating protein families. Cell. 1996;85(7):1047-55.
58. Constantin B. Dystrophin complex functions as a scaffold for signalling proteins. Biochim Biophys Acta. 2014;1838(2):635-42.
59. Liu XJ, Kong FZ, Wang YH, Zheng JH, Wan WD, Deng CL, et al. Lumican Accelerates Wound Healing by Enhancing alpha2beta1 Integrin-Mediated Fibroblast Contractility. PLoS One. 2013;8(6):e67124.
60. Greenhalgh DG. The role of growth factors in wound healing. J Trauma. 1996;41(1):159-67.
61. Steed DL. The role of growth factors in wound healing. Surg Clin North Am. 1997;77(3):575-86.
62. Barocas VH, Moon AG, Tranquillo RT. The fibroblast-populated collagen microsphere assay of cell traction force--Part 2: Measurement of the cell traction parameter. J Biomech Eng. 1995;117(2):161-70.
63. Li W, Hu X, Yang S, Wang S, Zhang C, Wang H, et al. A novel tissue-engineered 3D tumor model for anti-cancer drug discovery. Biofabrication. 2018;11(1):015004.
64. Koh I, Cha J, Park J, Choi J, Kang SG, Kim P. The mode and dynamics of glioblastoma cell invasion into a decellularized tissue-derived extracellular matrix-based three-dimensional tumor model. Sci Rep. 2018;8(1):4608.
65. Feng Y, Yang S, Ma Y, Bai XY, Chen X. Role of Toll-like receptors in diabetic renal lesions in a miniature pig model. Sci Adv. 2015;1(5):e1400183.
66. Cheng Y, Mansfield KJ, Sandow SL, Sadananda P, Burcher E, Moore KH. Porcine bladder urothelial, myofibroblast, and detrusor muscle cells: characterization and ATP release. Front Pharmacol. 2011;2:27.
67. Liao J, Joyce EM, Sacks MS. Effects of decellularization on the mechanical and structural properties of the porcine aortic valve leaflet. Biomaterials. 2008;29(8):1065-74.
68. Song JJ, Guyette JP, Gilpin SE, Gonzalez G, Vacanti JP, Ott HC. Regeneration and experimental orthotopic transplantation of a bioengineered kidney. Nat Med. 2013;19(5):646-51.
69. Piccoli M, D'Angelo E, Crotti S, Sensi F, Urbani L, Maghin E, et al. Decellularized colorectal cancer matrix as bioactive microenvironment for in vitro 3D cancer research. J Cell Physiol. 2018;233(8):5937-48.

70. Dunne LW, Huang Z, Meng W, Fan X, Zhang N, Zhang Q, et al. Human decellularized adipose tissue scaffold as a model for breast cancer cell growth and drug treatments. Biomaterials. 2014;35(18):4940-9.
71. Consolo F, Brizzola S, Tremolada G, Grieco V, Riva F, Acocella F, et al. A dynamic distention protocol for whole-organ bladder decellularization: histological and biomechanical characterization of the acellular matrix. J Tissue Eng Regen Med. 2016;10(2):E101-12.
72. Serrano-Aroca A, Vera-Donoso CD, Moreno-Manzano V. Bioengineering Approaches for Bladder Regeneration. Int J Mol Sci. 2018;19(6).
73. Chan YY, Sandlin SK, Kurzrock EA, Osborn SL. The Current Use of Stem Cells in Bladder Tissue Regeneration and Bioengineering. Biomedicines. 2017;5(1).
74. Xu Y, Fu W, Li G, Shi J, Tan H, Hu K, et al. Autologous urothelial cells transplantation onto a prefabricated capsular stent for tissue engineered ureteral reconstruction. J Mater Sci Mater Med. 2012;23(4):1119-28.
75. Zacharias M, Hunter KM, Luyk NH. Patient-controlled sedation using midazolam. Br J Oral Maxillofac Surg. 1994;32(3):168-73.
76. Bussard KM, Mutkus L, Stumpf K, Gomez-Manzano C, Marini FC. Tumor-associated stromal cells as key contributors to the tumor microenvironment. Breast Cancer Res. 2016;18(1):84.
77. Rosario DJ, Reilly GC, Ali Salah E, Glover M, Bullock AJ, Macneil S. Decellularization and sterilization of porcine urinary bladder matrix for tissue engineering in the lower urinary tract. Regen Med. 2008;3(2):145-56.
78. Hutmacher DW. Biomaterials offer cancer research the third dimension. Nat Mater. 2010;9(2):90-3.
79. Alemany-Ribes M, Semino CE. Bioengineering 3D environments for cancer models. Adv Drug Deliv Rev. 2014;79-80:40-9.
80. Ananthanarayanan B, Kim Y, Kumar S. Elucidating the mechanobiology of malignant brain tumors using a brain matrix-mimetic hyaluronic acid hydrogel platform. Biomaterials. 2011;32(31):7913-23.

Appendices

Appendix A.

Trial protocols: Decellularization by perfusion - kidney

Trial #1	dH_2O 500 mL 100 min.	1% Triton X-100 1000 mL 200 min.	1% Triton X-100 1000 mL 1000 min.	0.1% SDS 1000 mL 200 min.
Trial #2	dH_2O 500 mL 100 min.	1% Triton X-100 1000 mL 200 min.	1% Triton X-100 1000 mL 1000 min.	0.5% SDS 1000 mL 200 min.
Trial #3	dH_2O 1000 mL 200 min.	1% Triton X-100 2000 mL 400 min.	1% Triton X-100 1000 mL 1000 min.	0.1% SDS 1000 mL 200 min.
Trial #4	dH_2O 1000 mL 200 min.	0.6 M KCl 1000 mL 200 min.	1 M KI 1000 mL 200 min.	dH_2O 1000 mL 200 min.
Trial #5	dH_2O 1000 mL 200 min.	0.6 M KCl 2000 mL 400 min.	1 M KI 2000 mL 400 min.	dH_2O 1000 mL 200 min.

DNase I (2,000 unit) were perfused into the kidney at the end of decellularization cycles to eliminate remnant DNA fragments.

Appendix B

Trial protocols: Decellularization by immersion – urinary bladder

Trial #1	dH_2O 30 min.	1% Triton X-100 120 min.	0.1% SDS 120 min.	dH_2O overnight
Trial #2	dH_2O 30 min.	1% Triton X-100 180 min.	0.1% SDS 180 min.	dH_2O overnight
Trial #3	dH_2O 30 min.	1% Triton X-100 180 min.	0.5% SDS 180 min.	dH_2O overnight
Trial #4	dH_2O 30 min.	0.6 M KCl 120 min.	1 M KI 120 min.	dH_2O overnight
Trial #5	dH_2O 30 min.	0.6 M KCl 180 min.	1 M KI 180 min.	dH_2O overnight

All bladder immersion trials were tested in 50 mL centrifuge tube (Sigma-Aldrich, CLS40829, Damstadt, Germany), 150 mm x 25 mm tissue-culture treated culture dishes (Sigma-Aldrich, CLS430599, Damstadt, Germany) and 100 mm x 20 mm tissue-culture treated culture dishes (Sigma-Aldrich, CLS430167, Damstadt, Germany) respectively. DNase I (1kU/ml) were used at the end of immersion cycles to eliminate remnant DNA fragments.

Appendix C

Trial protocols: Decellularization by immersion – kidney

Trial #1	dH_2O 30 min.	1% Triton X-100 120 min.	0.1% SDS 120 min.	dH_2O overnight
Trial #2	dH_2O 30 min.	1% Triton X-100 180 min.	0.1% SDS 180 min.	dH_2O overnight
Trial #3	dH_2O 30 min.	1% Triton X-100 180 min.	0.5% SDS 180 min.	dH_2O overnight
Trial #4	dH_2O 30 min.	2% Triton X-100 180 min.	0.5% SDS 180 min.	dH_2O overnight
Trial #5	dH_2O 30 min.	0.6 M KCl 120 min.	1 M KI 120 min.	dH_2O overnight
Trial #6	dH_2O 30 min.	0.6 M KCl 180 min.	1 M KI 180 min.	dH_2O overnight

Appendix D

Trial protocols: Recellularization – kidney

	Number of cells	**Tissue Pre-immersed**	**Media used for recellularization**	**Timespan**
Trial #1	4,000	In FBS	Corresponding cell growth media	6 days
Trial #2	10,000	In FBS	Corresponding cell growth media	6 days
Trial #3	4,000	In corresponding growth media	Matrigel	21 days
Trial #4	10,000	In corresponding growth media	Matrigel	21 days
Trial #5	4,000	In corresponding growth media	Corresponding cell growth media	6 days

Appendix E

Trial protocols: Recellularization – Urinary bladder (single cell-type)

	Number of cells	**Tissue Pre-immersed**	**Media used for recellularization**	**Timespan**
Trial #1	1,000,000	In FBS	Corresponding cell growth media	6 days
Trial #2	500,000	In FBS	Corresponding cell growth media	6 days
Trial #3	1,000,000	In corresponding growth media	Matrigel	21 days
Trial #4	500,000	In corresponding growth media	Matrigel	21 days
Trial #5	1,000,000	In corresponding growth media	Corresponding cell growth media	6 days

Appendix F

Trial protocols: Recellularization – Urinary bladder (multi cell-type)

Total cell # = 5,000,000	**Ratio (HUVEC: Fibroblast: SV-HUC)**	**Tissue Pre-immersed**	**Media used for recellularization**	**Timespan**
Trial #1	1 :1 :1	In FBS	Corresponding cell growth media	6 days
Trial #2	2 :1 :2	In FBS	Corresponding cell growth media	6 days
Trial #3	1 :1 :1	In corresponding growth media	Matrigel	21 days
Trial #4	2 :1 :2	In corresponding growth media	Matrigel	21 days
Trial #5	2 :1 :2	In corresponding growth media	Corresponding cell growth media	6 days